NON-SMOOTH OPTIMIZATION FOR INTERFACE CRACKS IN COMPOSITE MATERIALS WITH NON-PENETRATION CONDITIONS

M. HINTERMÜLLER*, V.A. KOVTUNENKO†, AND K. KUNISCH◇

ABSTRACT. A constrained problem for a composite with an interface crack subject to non-penetration conditions is considered. The composite consisting of two identical homogeneous orthotropic materials is described with respect to an in-plane deformation. The coupling of the materials occurs at an interface with an angle of 2β between their vertical planes of elastic symmetry. The model is spatial, and we do not assume that it can be split into independent in-plane and anti-plane states. Well-posedness of the problem is proved by variational methods. For numerical computations a semi-smooth method is proposed and its convergence properties are studied. Based on the above model, we then describe a quasi-static delamination of the composite with a crack following the Griffith fracture criterion. This leads to a time-evolution problem for the (global) shape optimization of the total potential energy with respect to the crack length. Using the algorithms proposed in this paper, numerical experiments for an interface crack under mode-3 loading are presented and analyzed with respect to the half-angle β characterizing the coupling.

1. INTRODUCTION

Problems with cracks arise from applications in fracture mechanics and are of importance for the design of structures in the engineering sciences. A mathematical formulation of crack problems can be given within the framework of elasticity theory [23]. As a consequence of the presence of a crack in the domain singular solutions do occur. In the

1991 *Mathematics Subject Classification.* 49J40, 49M29, 73M05, 73C30.

Key words and phrases. Composite material, interface crack, variational methods, semi-smooth methods, constrained optimization, shape optimization.

* Department of Computational and Applied Mathematics - CAAM, Rice University, Houston, Texas, USA, and Department of Mathematics, University of Graz, Graz, Austria.

† Department of Mathematics, University of Graz, Graz, Austria, and Lavrent'ev Institute of Hydrodynamics, Novosibirsk, Russia.

◇ Department of Mathematics, University of Graz, Graz, Austria.

3-dimensional case these singularities are still subject of discussions. To gain some insight into the 3-dimensional situation, the standard approach is to simplify the elasticity model by splitting it into two 2-dimensional in-plane and anti-plane models. We point out that this leads to a loss of information concerning the 3-dimensional nature of the system. Motivated by these drawbacks, we introduce an intermediate 2.5-dimensional model instead of the splitting approach. Our model is a spatial one since it takes into account all 3 components of the displacement vector. However, it is formulated in a 2-dimensional domain.

For the construction of the 2.5-dimensional model we consider a homogeneous orthotropic material with a vertical plane of elastic symmetry rotated with an angle of β to a reference coordinate system. As a specific case, we consider a semi-isotropic material, which is fibered along a fixed direction having angle β with the x_3-axis and is isotropic in all cross-sections orthogonal to it. We compose two pieces of such a material along the interface given by the plane $x_2 = 0$ such that the corresponding angles in the upper and lower half-spaces are β and $-\beta$, respectively. We further assume that a crack is situated on part of the interface. Applying the assumption of plain deformation at $x_3 = const$, then, due to the rotation, this results in a spatial model. The formulation as a linear problem was suggested in [18].

In our numerical experiments we observe 3-dimensional effects: mixing of crack modes (mode-1 with mode-3), and mutual inter-penetration between opposite crack surfaces. They occur under pure mode-3 loading, which is ruled out for the in-plane and anti-plane models. Due to the latter phenomenon we are required to consider (unilaterally) constrained crack problems with non-penetration conditions. The inequality constraint imposed on the jump of the displacement at opposite crack faces prevents the non-physical, thus inconsistent, behavior of overlapping faces which can occur in the framework of the linear setting of the crack problem. The mathematical formulation results in a variational inequality. An account for the variational techniques can be found in [12, 13]. The variational formulation provides the appropriate state space for the crack problem which has a singularity at the crack tip.

For plane models the general approach to the analysis of singularities between two anisotropic half-planes was described in [27]. The elastic problem determinating the corresponding singular solutions can be reduced with the help of a partial Fourier transformation and the Stroh formalism to a matrix eigenvalue problem. An analytic realization of such a complicated technique is available for particular cases

only. Let us emphasize that the analytical solutions obtained in [27] require suitable orientation of the axes of material symmetry to ensure decoupling of the anti-plane fracture mode from the in-plane modes. Alternatively, in [24] (with no assumption of symmetry) an eigenvalue problem for power solutions (singular solutions of a specific form) was treated as a self-adjoint system to derive, in a formal way, the order of the singularity and to define its eigenvectors.

We shall investigate the geometric and physical features of the composite model by numerical experiments. For this purpose a semi-smooth Newton technique is adapted to constrained crack problems. As a rule, variational problems subject to unilateral constraints (the non-penetration conditions in our case) are not Fréchet differentiable with respect to the dual variable. This requires non-smooth optimization techniques [21, 14, 28]. Under suitable assumptions, semi-smoothness concepts will allow a locally super-linear convergence rate of the Newton iterates. Such properties are not available for problems with cracks due to the lack of regularity caused by the geometric singularities of a domain with a crack.

If we restrict our attention to the discretized problem, we arrive at a finite dimensional linear complementarity problem (see [3]). In this case superlinear convergence of the semi-smooth Newton method can be proved. Moreover, in numerical experiments global and monotone convergence was observed, which is supported by the *a posteriori* analysis in [8]. For a class of variational problems subject to boundary-constraints, in [9] we applied an argument based on perturbation of M-matrices guaranteeing these convergence properties.

Returning to the continuous setting of the problem, a penalization technique was utilized in [10] to obtain an approximate Lagrange multiplier, which enjoys extra L^p-regularity. As a consequence the generalized differentiability and the local super-linear convergence rate of the Newton iterates were derived for the penalized problem in function space.

For the problems under consideration semi-smooth Newton methods are equivalent to primal-dual active-set algorithms [7, 11]. They are an efficient tool for the numerical treatment of constrained variational problems. As suggested by the terminology, these algorithms use the primal as well as the dual variables independently to find the active (contact part of the crack surfaces) and the inactive (non-contact part) sets of the solution. In numerical examples the primal-dual active-set methods turned out to find the exact numerical solution in only a few (typically ≤ 12) iterations also in degenerate cases when pure primal methods may start to chatter. In comparison to interior-point

methods, see, *e.g.*, [20], the primal-dual active-set strategy determines not an approximate but the exact solution of the discrete problem. Decreasing the mesh-size results only in a moderate increase of the required number of iterations. Moreover, we suggest a combination of a local grid-refinement near the crack with a continuation technique reducing costly fine-grid iterations. For the numerical treatment of curvilinear cracks we refer to [22, 26], where extended finite element techniques are used.

One of the principal questions in fracture mechanics and structure design is to describe the stability properties of a solid with a crack and to predict its growth. By the Griffith fracture hypothesis the propagation of a crack is determined by the energy release rate at the crack tip, which cannot exceed a given physical parameter (see [2, 25]). A large number of papers investigated quasi-static growth of cracks in elastic media: [23, 6, 1, 17] etc. We argue that the energy release rate is the shape derivative of the potential energy functional with respect to variations of the crack tip. In [13, 12] methods of shape sensitivity analysis to crack problems with non-penetration conditions were adopted to provide a formula for the shape derivative. This includes the Griffith formula as a specific case.

We observe that the Griffith fracture criterion provides a necessary optimality condition for a local minimum (if it exists) of the total potential energy, which is defined as the sum of the potential and the surface energy. On the other hand, global shape optimization problems require minimization over all admissible crack shapes. For strictly convex cost functionals these two concepts coincide. In fracture mechanics this corresponds to stable crack propagation (progressive). The case of unstable (or brutal) crack growth is related to non-convex cost functionals. It was noticed in [5] that for brutal growth the Griffith fracture law (as a local criterion) predicts a critical loading for the initiation of crack propagation larger than that needed by the global optimization approach. This fact is observed in our numerical tests, too. By the global formulation of the shape optimization problem, not only continuous solutions for the stable crack propagation but also solutions with jumps and discontinuous velocities of the propagation are obtained.

Well-posedness properties for time-evolution problems with cracks were analyzed in [5, 4]. In the present work we apply the global formulation of the problem of shape optimization to a rectilinear crack and utilize it on a set of local minimizers derived in a constructive way from the Griffith fracture law. Note that the delamination process suggests a predefined path (along the interface) of the crack time-evolutions,

which was confirmed experimentally [15]. This problem is solved numerically to describe the delamination of composite materials with an interface crack under quasi-static linear loading. For this purpose we adopt the primal-dual active set method introduced for the solution of the constrained state problem.

The paper consists of three parts: Section 2 serves for the formulation of the problem, Section 3 deals with its numerical treatment, and Section 4 describes the shape optimization for the state problem.

2. Constrained crack problems for a composite

In this section we formulate a model with respect to an in-plane deformation for two identical homogeneous orthotropic materials, which are composed at a planar interface with the angle of 2β between their vertical planes of elastic symmetry and which have a crack along a part of their interface. The specific cases of material parameters for fibered, isotropic, and orthotropic solids are described in the Appendix. Based on the corresponding representation of elasticity coefficients, on constitutive and equilibrium laws, we deduce the variational setting of the problem.

2.1. **Modeling of composite materials in plane deformation.**

Consider a homogeneous orthotropic material with planes of elastic symmetry corresponding to the (x_1', x_2', x_3')-axes, which can be described by 9 independent (positive) material parameters (see [19]):

$$E_1,\ E_2,\ E_3,\ \nu_{21},\ \nu_{32},\ \nu_{31},\ G_{21},\ G_{32},\ G_{31}. \tag{2.1}$$

First, we compose the identical materials with respect to a reference coordinate system (x_1, x_2, x_3) in the following way. In the "upper" half-space $\mathbb{R}^3_+ = \{x_1, x_2 \geq 0, x_3\}$ the (x_1', x_2', x_3')-axes are rotated in the anti-clockwise direction to (x_1, x_2, x_3) with respect to the common $x_2' = x_2$-axis by the angle β between x_3' and x_3. The angle $\beta \in [-\pi/2, \pi/2]$ is arbitrarily fixed. In the "lower" half-space $\mathbb{R}^3_- = \{x_1, x_2 \leq 0, x_3\}$ the (x_1', x_2', x_3')-axes are rotated to (x_1, x_2, x_3) with respect to $x_2' = x_2$ in the opposite direction by the same angle (*i.e.*, $-\beta$), as it is illustrated in Figure 1. The materials are assumed to be joined along the plane $x_2 = 0$ with an interface defect (crack).

For a displacement vector $u = (u_1, u_2, u_3)^\top(x)$ (at a point $x = (x_1, x_2, x_3)^\top \in \mathbb{R}^3$) in the composite material

$$u = \begin{cases} u^+ & \text{in } \mathbb{R}^3_+, \\ u^- & \text{in } \mathbb{R}^3_-, \end{cases}$$

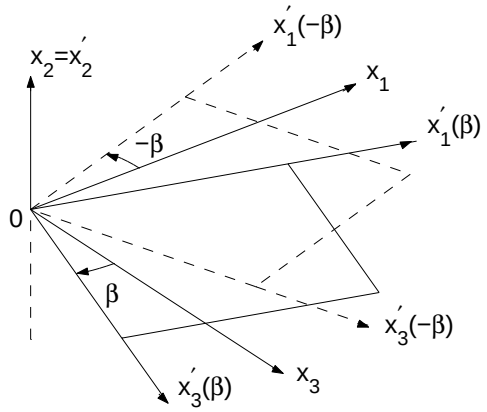

FIGURE 1. Composing of a body in $\mathbb{R}^3_{\pm}$.

we introduce a strain tensor $\varepsilon = \{\varepsilon_{ij}\}$ according to the linear Cauchy law

$$\varepsilon_{ij}(u) = 0.5(u_{i,j} + u_{j,i}), \quad i,j = 1,2,3, \tag{2.2}$$

and a 3×3 symmetric tensor of stress $\sigma = \{\sigma_{ij}\}$ as

$$\sigma(u) = \begin{cases} \sigma^{\beta}(u^+) & \text{in } \mathbb{R}^3_+, \\ \sigma^{-\beta}(u^-) & \text{in } \mathbb{R}^3_-. \end{cases} \tag{2.3}$$

Here and throughout we utilize the standard tensor notation common in linear elasticity and the summation convention for the repeated indices $i,j = 1,2,3$.

Second, we apply the assumption of plane deformation at every cross-section $x_3 = const$, which means that all three components of the displacement vector u do not depend on x_3. Hence $\varepsilon_{33} = 0$ and the strain tensor in (2.2) takes the particular form

$$\begin{aligned} &\varepsilon_{11}(u) = u_{1,1}, \quad \varepsilon_{22}(u) = u_{2,2}, \\ &\varepsilon_{12}(u) = 0.5(u_{1,2} + u_{2,1}), \\ &\varepsilon_{13}(u) = 0.5u_{3,1}, \quad \varepsilon_{23}(u) = 0.5u_{3,2}. \end{aligned} \tag{2.4}$$

In $\mathbb{R}^3_+$, the relevant components of the stress tensor (2.3) satisfy the following constitutive relations involving a non-symmetric matrix:

$$\begin{bmatrix} \sigma^\beta_{11} \\ \sigma^\beta_{22} \\ \sigma^\beta_{12} \\ \sigma^\beta_{23} \\ \sigma^\beta_{13} \end{bmatrix} = \begin{bmatrix} C^\beta_{11} & C^\beta_{12} & 0 & 0 & 2C^\beta_{16} \\ C^\beta_{12} & C_{22} & 0 & 0 & 2C^\beta_{26} \\ 0 & 0 & 2C^\beta_{44} & 2C^\beta_{45} & 0 \\ 0 & 0 & 2C^\beta_{45} & 2C^\beta_{55} & 0 \\ C^\beta_{16} & C^\beta_{26} & 0 & 0 & 2C^\beta_{66} \end{bmatrix} \begin{bmatrix} \varepsilon_{11} \\ \varepsilon_{22} \\ \varepsilon_{12} \\ \varepsilon_{23} \\ \varepsilon_{13} \end{bmatrix} \tag{2.5}$$

with 9 elasticity coefficients depending on β (except for C_{22}) and the material parameters (2.1) as presented in the Appendix. The substitution of (2.4) into (2.5) allows us to rewrite the constitutive law in the symmetric form:

$$\begin{aligned} \sigma^\beta_{11}(u) &= C^\beta_{11}u_{1,1} + C^\beta_{12}u_{2,2} + C^\beta_{16}u_{3,1}, \\ \sigma^\beta_{22}(u) &= C^\beta_{12}u_{1,1} + C_{22}u_{2,2} + C^\beta_{26}u_{3,1}, \\ \sigma^\beta_{12}(u) &= C^\beta_{44}(u_{1,2} + u_{2,1}) + C^\beta_{45}u_{3,2}, \\ \sigma^\beta_{23}(u) &= C^\beta_{45}(u_{1,2} + u_{2,1}) + C^\beta_{55}u_{3,2}, \\ \sigma^\beta_{13}(u) &= C^\beta_{16}u_{1,1} + C^\beta_{26}u_{2,2} + C^\beta_{66}u_{3,1}. \end{aligned} \tag{2.6}$$

In $\mathbb{R}^3_-$ the above relations hold true if we exchange β with $-\beta$ according to (2.3). The elasticity coefficients obey the following symmetry properties (see the Appendix):

$$\begin{aligned} &C^{-\beta}_{11} = C^\beta_{11},\ C^{-\beta}_{12} = C^\beta_{12},\ C^{-\beta}_{44} = C^\beta_{44},\ C^{-\beta}_{55} = C^\beta_{55},\ C^{-\beta}_{66} = C^\beta_{66}, \\ &C^{-\beta}_{16} = -C^\beta_{16},\ C^{-\beta}_{26} = -C^\beta_{26},\ C^{-\beta}_{45} = -C^\beta_{45}. \end{aligned} \tag{2.7}$$

Note that if $\beta = 0$ or $\beta = \pm\pi/2$ then we have $C^\beta_{16} = C^\beta_{26} = C^\beta_{45} = 0$ and (2.6) is split into two independent states, namely the in-plane state for $(u_1, u_2)^\top$ and the anti-plane state for u_3. If $\beta \neq 0, \pm\pi/2$ then we have a spatial model.

2.2. **Equilibrium problem for the interface crack with non-penetration conditions.** Consider the composite of two elastic orthotropic materials joined along the plane $x_2 = 0$, which was described in Section 2.1. Assume that in each cross-section with $x_3 = const$ the solid occupies a domain $\Omega \subset \mathbb{R}^2$ consisting of two sub-domains $\Omega^+ \subset \mathbb{R}^2_+$ and $\Omega^- \subset \mathbb{R}^2_-$ with the interface Σ located on the line $x_2 = 0$, *i.e.*, $\Omega = \Omega^+ \cup \Omega^- \cup \Sigma$. Let Ω be bounded by the Lipschitz boundary $\partial\Omega = \Gamma_N \cup \Gamma_D$ with an outward normal vector $n = (n_1, n_2)^\top$, where $\Gamma_D \neq \emptyset$. We suppose that the crack Γ_C is a part of the interface Σ and define the domain with the crack as $\Omega_C = \Omega \setminus \overline{\Gamma}_C$. Its boundary $\partial\Omega_C$ is the union of Γ_N, Γ_D, and the crack surfaces $\Gamma^\pm_C$. Here $\Gamma^+_C \subset \Sigma^+$

and $\Gamma_C^- \subset \Sigma^-$ are defined as the limit points of sequences $(x) \in \Omega^+$ and $(x) \in \Omega^-$ at Σ, respectively.

To prevent mutual inter-penetrations between the opposite crack surfaces Γ_C^+ and Γ_C^- we impose a non-negativity condition on the jump of the displacement normal to the crack (u_2-component), see [12]. Let $g = (g_1, g_2, g_3)^\top$ represent a surface traction given at Γ_N, and, without loss of generality, assume that the volume force is zero. Further, the solid is assumed to be fixed at Γ_D. The problem of equilibrium of the composite with a crack is finally described by the following non-linear (at Γ_C) relations:

$$
\begin{aligned}
-\sigma_{1\alpha,\alpha}(u) = -\sigma_{2\alpha,\alpha}(u) = -\sigma_{3\alpha,\alpha}(u) = 0 \quad & \text{in } \Omega_C, \\
\sigma_{12}(u) = \sigma_{23}(u) = 0 \quad & \text{on } \Gamma_C^{\pm}, \\
[\![\sigma_{22}(u)]\!] = 0,\ [\![u_2]\!] \geq 0,\ \sigma_{22}(u) \leq 0,\ \sigma_{22}(u)[\![u_2]\!] = 0 \quad & \text{on } \Gamma_C, \\
[\![u_1]\!] = [\![u_2]\!] = [\![u_3]\!] = 0, & \\
[\![\sigma_{12}(u)]\!] = [\![\sigma_{22}(u)]\!] = [\![\sigma_{23}(u)]\!] = 0 \quad & \text{on } \Sigma \setminus \Gamma_C, \\
\sigma_{1\alpha}(u)n_\alpha = g_1,\ \sigma_{2\alpha}(u)n_\alpha = g_2,\ \sigma_{3\alpha}(u)n_\alpha = g_3 \quad & \text{on } \Gamma_N, \\
u_1 = u_2 = u_3 = 0 \quad & \text{on } \Gamma_D,
\end{aligned}
\tag{2.8}
$$

where the summation convention over repeated indices $\alpha = 1, 2$ is used. Here $[\![u]\!] = u^+ - u^-$ and $[\![\sigma(u)]\!] = \sigma^\beta(u^+) - \sigma^{-\beta}(u^-)$ denote the jumps across the interface.

In view of (2.6) and (2.7) the divergence of the stress used in (2.8) has the following representation in $\Omega_C^{\pm}$:

$$
\begin{aligned}
\sigma^{\pm\beta}_{1\alpha,\alpha}(u^\pm) &= C^\beta_{11}u^\pm_{1,11} + C^\beta_{44}u^\pm_{1,22} + (C^\beta_{12} + C^\beta_{44})u^\pm_{2,12} \\
&\quad \pm C^\beta_{16}u^\pm_{3,11} \pm C^\beta_{45}u^\pm_{3,22}, \\
\sigma^{\pm\beta}_{2\alpha,\alpha}(u^\pm) &= (C^\beta_{12} + C^\beta_{44})u^\pm_{1,12} + C^\beta_{44}u^\pm_{2,11} + C_{22}u^\pm_{2,22} \\
&\quad \pm (C^\beta_{45} + C^\beta_{26})u^\pm_{3,12}, \\
\sigma^{\pm\beta}_{3\alpha,\alpha}(u^\pm) &= \pm C^\beta_{16}u^\pm_{1,11} \pm C^\beta_{45}u^\pm_{1,22} \pm (C^\beta_{45} + C^\beta_{26})u^\pm_{2,12} \\
&\quad + C^\beta_{66}u^\pm_{3,11} + C^\beta_{55}u^\pm_{3,22}.
\end{aligned}
\tag{2.9}
$$

2.3. **Constrained variational problem with a crack.** We introduce the cone of admissible displacements which accounts for all the boundary conditions imposed on u in (2.8) as

$$
\begin{aligned}
K(\Omega_C) &= \{u \in H(\Omega_C) : \quad [\![u_2]\!] \geq 0 \quad \text{on } \Gamma_C\} \quad \text{with} \\
H(\Omega_C) &= \{u \in H^1(\Omega_C)^3 : \quad u = 0 \quad \text{on } \Gamma_D\}.
\end{aligned}
$$

For given $g \in L^2(\Gamma_N)^3$ the potential energy of the composite with a crack is defined by

$$\Pi(u) = \frac{1}{2}\int_{\Omega_C} \sigma_{ij}(u)\varepsilon_{ij}(u)\,dx - \int_{\Gamma_N} g_i u_i\,ds, \tag{2.10}$$

where due to (2.4), (2.6), and (2.7) the quadratic form has the representation in $\Omega_C^{\pm}$ (recall that $\varepsilon_{33} = 0$):

$$\begin{aligned}\sigma_{ij}^{\pm\beta}(u^{\pm})\varepsilon_{ij}(u^{\pm}) &= C_{11}^{\beta}(u_{1,1}^{\pm})^2 + C_{22}(u_{2,2}^{\pm})^2 + 2C_{12}^{\beta}u_{1,1}^{\pm}u_{2,2}^{\pm}\\ &\pm 2C_{16}^{\beta}u_{1,1}^{\pm}u_{3,1}^{\pm} \pm 2C_{26}^{\beta}u_{2,2}^{\pm}u_{3,1}^{\pm} + C_{44}^{\beta}(u_{1,2}^{\pm} + u_{2,1}^{\pm})^2\\ &\pm 2C_{45}^{\beta}(u_{1,2}^{\pm} + u_{2,1}^{\pm})u_{3,2}^{\pm} + C_{55}^{\beta}(u_{3,2}^{\pm})^2 + C_{66}^{\beta}(u_{3,1}^{\pm})^2.\end{aligned} \tag{2.11}$$

The weak solution $u \in K(\Omega_C)$ to the equilibrium problem (2.8) is defined as the solution to the constrained minimization problem

$$\text{minimize } \Pi(v) \quad \text{over } v \in K(\Omega_C). \tag{2.12}$$

The optimality condition to (2.12) is expressed by the variational inequality

$$\int_{\Omega_C} \sigma_{ij}(u)\varepsilon_{ij}(v-u)\,dx \geq \int_{\Gamma_N} g_i(v-u)_i\,ds \quad \text{for all } v \in K(\Omega_C). \tag{2.13}$$

For unique solvability of (2.12) (or, equivalently (2.13)) uniform positivity of the quadratic term is needed, *i.e.*, the existence of an angle β and a constant $c_0(\beta) > 0$ such that

$$\int_{\Omega_C} \sigma_{ij}(u)\varepsilon_{ij}(u)\,dx \geq c_0(\beta)\|u\|^2_{H(\Omega_C)} \quad \text{for every } u \in H(\Omega_C) \tag{2.14}$$

holds. Note that condition (2.14) may not be true for all $\beta \in [-\pi/2, \pi/2]$. If the 5×5-matrix in (2.6) is positive definite for some β, then this leads to the estimate:

$$\int_{\Omega_C} \sigma_{ij}(u)\varepsilon_{ij}(u)\,dx \geq \lambda_{min}(\beta)\int_{\Omega_C} \varepsilon_{ij}(u)\varepsilon_{ij}(u)\,dx \tag{2.15}$$

with the minimal eigenvalue $\lambda_{min}(\beta) > 0$ of this matrix. In this case, a Korn-type argument based on (2.15) implies (2.14).

It can be verified for the solution u of (2.13) that $[\![u]\!] \in H_{00}^{1/2}(\Gamma_C)^3$, where $H_{00}^{1/2}(\Gamma_C)$ is the space of functions in $H^{1/2}(\Gamma_C)$ which admit a continuation by zero on an extension of Γ_C into Ω_C. Since the trace of

$H(\Omega_C)$ onto $H^{1/2}_{00}(\Gamma_C)^3$ is surjective there exists a Lagrange multiplier $\lambda \in H^{1/2}_{00}(\Gamma_C)^\star$ such that

$$\int_{\Omega_C} \sigma_{ij}(u)\varepsilon_{ij}(v)\,dx - \langle \lambda, [\![v_2]\!]\rangle_{\Gamma_C} = \int_{\Gamma_N} g_i v_i\,ds \text{ for all } v \in H(\Omega_C), \tag{2.16a}$$

$$\langle \lambda, \xi - [\![u_2]\!]\rangle_{\Gamma_C} \geq 0 \quad \text{for all } 0 \leq \xi \in H^{1/2}_{00}(\Gamma_C), \tag{2.16b}$$

where $\langle\,\cdot\,,\,\cdot\,\rangle_{\Gamma_C}$ stands for the duality pairing between the spaces $H^{1/2}_{00}(\Gamma_C)$ and $H^{1/2}_{00}(\Gamma_C)^\star$. Applying Green's formula to the first term in (2.13) and using (2.16a) we arrive at the identity

$$\sigma^{\beta}_{22}(u^+) = \sigma^{-\beta}_{22}(u^-) = -\lambda \quad \text{on } \Gamma_C^{\pm}. \tag{2.17}$$

Thus (2.16) yields the primal-dual variational formulation of the equilibrium problem (2.8). Note that it expresses an optimality condition for the minimization of the Lagrangian

$$L(u,\lambda) = \frac{1}{2}\int_{\Omega_C} \sigma_{ij}(u)\varepsilon_{ij}(u)\,dx - \langle \lambda, [\![u_2]\!]\rangle_{\Gamma_C} - \int_{\Gamma_N} g_i u_i\,ds$$

over all admissible pairs $(u,\lambda)^\top \in H(\Omega_C) \times H^{1/2}_{00}(\Gamma_C)^\star$ subject to the dual constraint $\lambda \geq 0$, which is understood in the generalized sense.

2.4. **Numerical example.** Before starting a discretization of the problem and describing a numerical algorithm for its solution we give an illustrative example. It clarifies principal features of the system under consideration.

We choose the following symmetric geometry for the composite with a crack as presented in Figure 2. The domain Ω is chosen to be a square in $\mathbb{R}^2$ with its boundary decomposed as follows:

$$\Gamma_D = \{x_1 = 1, |x_2| \leq 0.5\}, \quad \Gamma_N = \Gamma^+_{N1} \cup \Gamma^-_{N1} \cup \Gamma^+_{N2} \cup \Gamma^-_{N2},$$
$$\Gamma^{\pm}_{N1} = \{x_1 = 0, 0 \leq \pm x_2 \leq 0.5\}, \quad \Gamma^{\pm}_{N2} = \{0 < x_1 < 1, x_2 = \pm 0.5\}.$$

We assume that the crack Γ_C of length $0 < l < L = 1$ is located along a part of the interface $\Sigma = \{0 < x_1 < 1, x_2 = 0\}$. The corresponding faces in $\Omega^{\pm} = \Omega \cap \mathbb{R}^2_{\pm}$ of the crack and the interface are denoted by $\Gamma_C^{\pm}$ and $\Sigma^{\pm}$, respectively. The plane domain with crack Ω_C is bounded by Γ_D, Γ_N, and $\Gamma_C^{\pm}$. The elastic problem (2.8) in Ω_C is considered with the following boundary conditions imposed on Γ_N:

$$\begin{aligned} \sigma_{12}(u) = \sigma_{22}(u) = \sigma_{23}(u) = 0 \quad &\text{on } \Gamma^{\pm}_{N2}, \\ -\sigma_{11}(u) = g^{\pm}_1,\ -\sigma_{12}(u) = g^{\pm}_2,\ -\sigma_{13}(u) = g^{\pm}_3 \quad &\text{on } \Gamma^{\pm}_{N1}, \end{aligned} \tag{2.18}$$

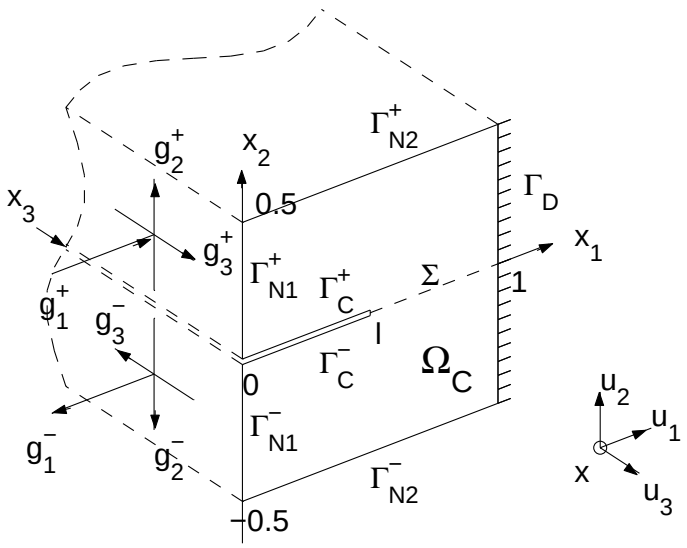

FIGURE 2. Geometry of domain Ω_C.

where we assume anti-symmetric loading corresponding to mode-3:

$$g_3^{\pm} = \mp g_0, \quad g_1^{\pm} = g_2^{\pm} = 0, \quad g_0 = 0.001\mu \approx 3.5376(\text{mPa}), \tag{2.19}$$

as illustrated in Figure 2.

We utilize the material parameters (2.1) for the specific case (5.3) described in the Appendix with the values from [15]:

$$E_1 = E_2 = E = 10160(\text{mPa}),\ E_3 = 139400(\text{mPa}),$$

$$G_{31} = G_{32} = G_3 = 4600(\text{mPa}),\ G_{21} = \frac{E}{2(1+\nu)} \approx 3537.6(\text{mPa}),$$

$$\nu_{21} = \nu = 0.436,\ \nu_{31} = \nu_{32} = \nu_3 = 0.3.$$

The corresponding minimal eigenvalues $\lambda_{min}(\beta)$ in (2.15) are found to be positive for $\beta \in [-\pi/2, \pi/2]$. They are approximately constant with value $\lambda_{min} \approx 3537.6$. In this case (2.14) holds, and the interface crack problem formulated in Section 2.3 is well-posed.

For calculations, the angle β of fibering is taken at the six points $\beta = 0, \pi/16, \pi/8, \pi/4, 3\pi/8, \pi/2$ in $[0, \pi/2]$. This includes the limit cases of the plane isotropic model with $\beta = 0$, and the plane orthotropic model with $\beta = \pi/2$. Note that for $\beta = \pi/4$ the directions of fibering in Ω_C^+ and Ω_C^- are orthogonal to each other.

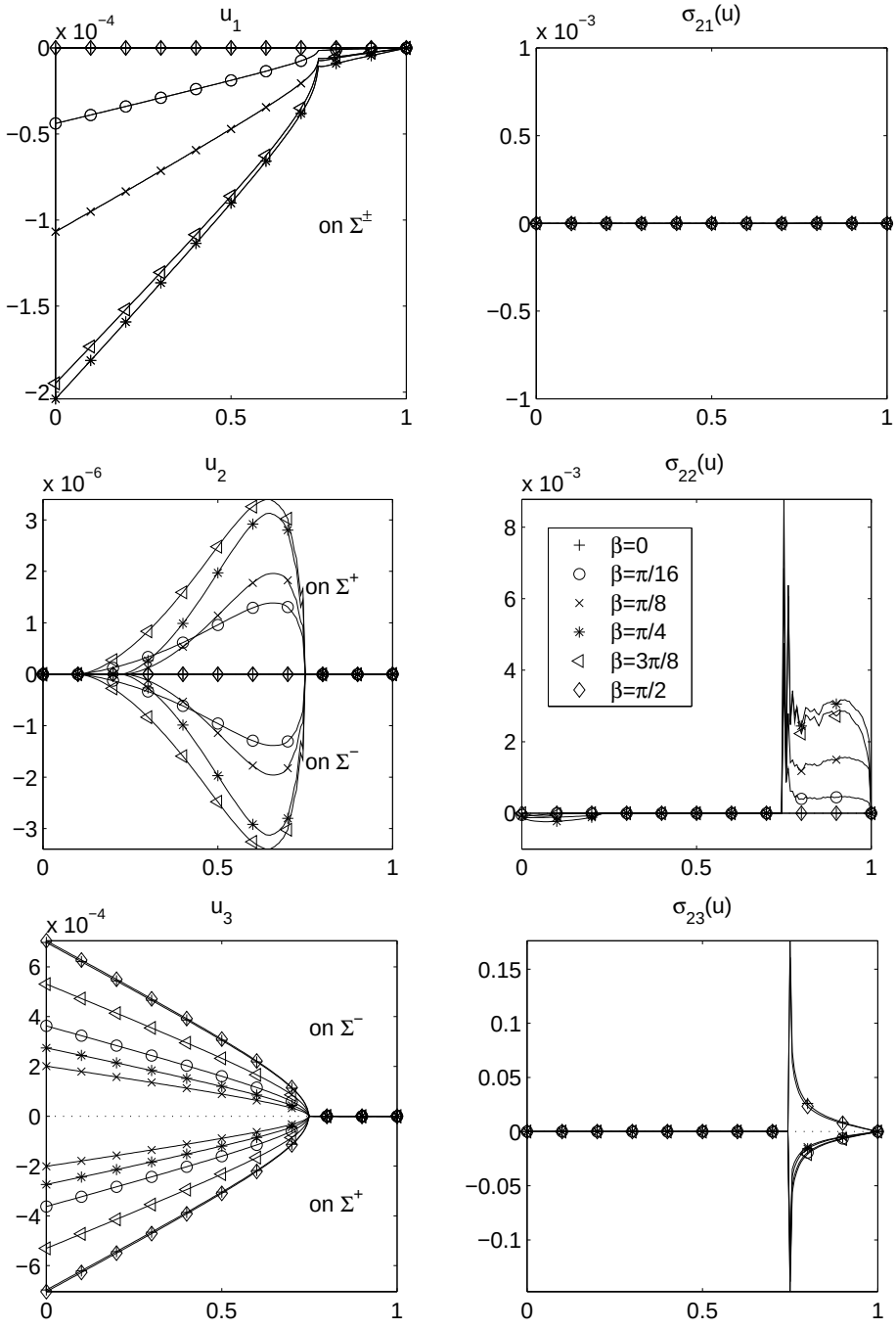

FIGURE 3. Displacement and stress at interface.

For $l = 0.75$ the components of displacements u_1, u_2, u_3 and the stresses $\sigma_{12}(u)$, $\sigma_{22}(u)$, $\sigma_{23}(u)$ at the interface surfaces $\Sigma^{\pm}$ are depicted

in Figure 3 for various fibering angles β. We observe in Figure 3 the following behavior:

- $[\![u_1]\!] = 0$ on Σ and $[\![u_3]\!] < 0$ on Γ_C for all β; $u_1 = u_2 = 0$ for $\beta = 0, \pi/2$; $u_1 < 0$ and $[\![u_2]\!] \geq 0$ on Γ_C for $\beta = \pi/16, \pi/8, \pi/4, 3\pi/8$.
- $\sigma_{21}(u) = 0$ on Σ, $\sigma_{23}(u)$ has a r^{-c}-singularity at the crack tip for all β; $\sigma_{22}(u) = 0$ for $\beta = 0, \pi/2$ and otherwise $\sigma_{22}(u) \neq 0$ and it has a r^{-c}-singularity.

This case indicates clearly the appearance of a mixed mode-1 ($[\![u_2]\!] \neq 0$) and mode-3 ($[\![u_3]\!] \neq 0$) crack under pure mode-3 loading. Moreover, contact between opposite crack surfaces occurs. This situation is related to the 3-dimensional elasticity state and shows the advantage of the spatial model with non-penetration conditions, in contrast to plane isotropic ($\beta = 0$) and orthotropic ($\beta = \pi/2$) models.

Note that there is no contact between the crack surfaces in the remaining interval $\beta \in (-\pi/2, 0)$. This case was investigated in [18] for the linear setting of the problem with the condition $\sigma_{22}(u) = 0$ describing stress-free crack faces $\Gamma_C^{\pm}$.

3. Constrained minimization of the discrete crack problem

For the numerical treatment of the constrained variational problem with interface cracks in the composite, we rely on the following *semi-smoothness* concept. The operator $F : X \to Y$, with X, Y Banach spaces is called generalized differentiable in an open subset $U \subset X$ if there exists mappings $G : U \to \mathcal{L}(X, Y)$, referred to as generalized derivatives, such that

$$\lim_{h \to 0} \frac{1}{\|h\|_X} \|F(y+h) - F(y) - G(y+h)h\|_Y = 0 \quad \text{for every } y \in U.$$

In this section we use this property in $\mathbb{R}^N$ and construct the resulting semi-smooth Newton algorithm.

3.1. Discretized problem as linear complementarity system.

Discretization of (2.12) results in a quadratic programming problem of the type

$$\text{minimize } \frac{1}{2} u^\top L u - f^\top u \quad \text{over } u \in \mathbb{R}^N \quad \text{subject to } \Lambda u \geq 0, \tag{3.1}$$

where the symmetric matrix $L \in \mathbb{R}^{N \times N}$ is positive-definite, $f \in \mathbb{R}^N$, and the matrix $\Lambda \in \mathbb{R}^{|B| \times N}$ associated to the non-penetration conditionhas full column-rank. Here, for the index set $B \subset \{1, \ldots, N\}$ we denote by $|B|$ its cardinality. The form of Λ for the specific case of a

symmetric partition of the crack surfaces is presented in the numerical examples below.

It is well-known that the unique solution $u \in \mathbb{R}^N$ to (3.1) exists and is characterized by the variational inequality (similar to (2.13))

$$\Lambda u \geq 0, \quad (f - Lu)^\top (v - u) \leq 0 \quad \text{for all } v \in \mathbb{R}^N \text{ with } \Lambda v \geq 0. \tag{3.2}$$

Introducing a Lagrange multiplier $\lambda \in \mathbb{R}^{|B|}$ we can equivalently express problem (3.1) as: Find the pair $(u, \lambda)^\top \in \mathbb{R}^N \times \mathbb{R}^{|B|}$ satisfying the following system of equations (compare with (2.16))

$$Lu - \Lambda^\top \lambda = f, \tag{3.3a}$$

$$\Phi(u, \lambda) := \max(c\lambda - \Lambda u, 0) - c\lambda = 0, \tag{3.3b}$$

where $c > 0$ is an arbitrarily fixed constant. Note that (3.3) is also sufficient for the primal variable u to be the solution of (3.2) and (3.1).

Multiplying (3.3a) first by L^{-1} and then by Λ we obtain

$$\Lambda u - (\Lambda L^{-1} \Lambda^\top)\lambda - \Lambda L^{-1} f = 0. \tag{3.4}$$

Since the matrix $\Lambda L^{-1} \Lambda^\top$ is positive definite we can define its inverse (which is a positive definite matrix again)

$$\hat{L} := (\Lambda L^{-1} \Lambda^\top)^{-1} \in \mathbb{R}^{|B| \times |B|}. \tag{3.5}$$

Setting

$$\hat{u} := \Lambda u \in \mathbb{R}^{|B|}, \quad \hat{f} := \hat{L} \Lambda L^{-1} f \in \mathbb{R}^{|B|}, \tag{3.6}$$

multiplying (3.4) by $\hat{L}$, and taking (3.3b) into account we arrive at the linear complementarity problem for $\hat{u}$ at the subset of indices B only: Find $\hat{u} \in \mathbb{R}^{|B|}$ such that

$$\hat{L}\hat{u} - \hat{f} \geq 0, \quad \hat{u} \geq 0, \quad \hat{u}^\top (\hat{L}\hat{u} - \hat{f}) = 0. \tag{3.7}$$

This is the first order necessary and sufficient optimality condition for the strictly convex quadratic minimization problem

$$\text{minimize } \frac{1}{2} \hat{u}^\top \hat{L} \hat{u} - \hat{f}^\top \hat{u} \quad \text{over } \hat{u} \in \mathbb{R}^{|B|} \text{ subject to } \hat{u} \geq 0, \tag{3.8}$$

which admits a unique solution $\hat{u}$. Let $\hat{\lambda}$ denote the multiplier associated to (3.8). Then the pair $(\hat{u}, \hat{\lambda})^\top \in \mathbb{R}^{|B|} \times \mathbb{R}^{|B|}$ satisfies the non-linear equations analogous to (3.3):

$$\hat{L}\hat{u} - \hat{\lambda} = \hat{f}, \tag{3.9a}$$

$$\hat{\Phi}(\hat{u}, \hat{\lambda}) := \max(c\hat{\lambda} - \hat{u}, 0) - c\hat{\lambda} = 0, \tag{3.9b}$$

with an arbitrarily fixed $c > 0$.

Lemma 3.1. *Let* $(u,\lambda)^\top \in \mathbb{R}^N \times \mathbb{R}^{|B|}$ *be the solution to* (3.3). *Then* $\hat{u} = \Lambda u$ *and* $\hat{\lambda} = \lambda$ *solve* (3.9). *Conversely, let* $(\hat{u},\hat{\lambda})^\top \in \mathbb{R}^{|B|} \times \mathbb{R}^{|B|}$ *be the solution to* (3.9), *then*

$$u = L^{-1}(f + \Lambda^\top \hat{\lambda}) \tag{3.10}$$

and $\lambda = \hat{\lambda}$.

Proof. The first assertion of the lemma follows from the discussion above (3.9). To verify the converse assertion, multiplying (3.9a) by $\hat{L}^{-1}$ yields

$$\hat{u} - (\Lambda L^{-1}\Lambda^\top)\hat{\lambda} - \Lambda L^{-1} f = 0.$$

From (3.10) and (3.9) we obtain

$$Lu - f - \Lambda^\top \hat{\lambda} = 0, \quad \Lambda u = \hat{u} \geq 0, \quad \hat{\lambda} \geq 0,$$

which (similarly to (3.7)) is the linear complementarity problem associated to (3.3). Now the claim follows from the uniqueness of the solution to (3.3). □

This equivalence will be useful for the application of the convergence results of [9, 10].

3.2. **The primal-dual active-set algorithm as a semi-smooth Newton method.** In order to devise a semi-smooth Newton method for solving the constrained minimization problem (3.1) we focus on its primal-dual formulation (3.3). Setting $y := (u,\lambda)^\top \in \mathbb{R}^N \times \mathbb{R}^{|B|}$ we restate the system (3.3) as

$$F(y) := \begin{pmatrix} Lu - \Lambda^\top \lambda - f \\ \Phi(u,\lambda) \end{pmatrix} = 0, \tag{3.11}$$

where the function $F : \mathbb{R}^{N+|B|} \to \mathbb{R}^{N+|B|}$ is non-differentiable in the classical sense. However, in the sequel we argue that F is generalized differentiable. For this purpose we introduce the matrix $\chi_S \in \mathbb{R}^{|B|\times|B|}$ by

$$\chi_S = \operatorname{diag}(s_1,\ldots,s_{|B|}), \quad \text{with } s_i = \begin{cases} 1 & \text{if } i \in S, \\ 0 & \text{if } i \notin S, \end{cases}$$

and we define

$$\begin{aligned} A(y) &= \{i \in B : c\lambda_i - (\Lambda u)_i > 0\}, \\ I(y) &= \{i \in B : c\lambda_i - (\Lambda u)_i \leq 0\}. \end{aligned} \tag{3.12}$$

The set $A(y)$ is called the *active* set at y, and $I(y)$ is called the *inactive* set. This terminology is suggested by the fact that $\lambda_i > 0$ and $(\Lambda u)_i = 0$ for all $i \in A(y)$ at the solution y of (3.3). On the other hand, for $i \in I(y)$ we have $\lambda_i = 0$ and $(\Lambda u)_i \geq 0$ at the solution. Definition

(3.12) implies that $\chi_{A(y)} + \chi_{I(y)} = 1$. This allows us to rewrite the function Φ in (3.3b) in the form

$$\Phi(u, \lambda) = -\chi_{A(y)}\Lambda u - c\chi_{I(y)}\lambda. \tag{3.13}$$

As a consequence, F in (3.11) admits the representation

$$F(y) = G(y)y - \begin{pmatrix} f \\ 0 \end{pmatrix}, \quad G(y) = \begin{pmatrix} L & -\Lambda^\top \\ -\chi_{A(y)}\Lambda & -c\chi_{I(y)} \end{pmatrix},$$

and satisfies, for small h, the identity

$$F(y + h) - F(y) - G(y + h)h = 0. \tag{3.14}$$

Thus, G in (3.14) serves as a generalized derivative of the non-differentiable mapping F.

Now we can define the semismooth Newton method for computing the solution to (3.11): For some initial guess $y^{(0)}$ compute

$$y^{(n+1)} = y^{(n)} - G(y^{(n)})^{-1}F(y^{(n)}), \quad n = 0, 1, \ldots. \tag{3.15}$$

As we shall detail below, each step in (3.15) amounts to solving a well-posed linear system. From [7, Theorem 1.1] the following local convergence result for the process (3.15) can be deduced.

Proposition 3.1. *The semismooth Newton iteration* (3.15) *is well-defined, and the sequence of iterates* $(y^{(n)})$ *converges superlinearly to a solution* y^* *of* $F(y) = 0$ *provided that* $y^{(0)}$ *is sufficiently close to* y^*.

The numerical implementation of (3.15) is realized as follows.

Algorithm 1.

(0) *Choose* $A(y^{(-1)})$ *and* $I(y^{(-1)})$ *such that* $A(y^{(-1)}) \cup I(y^{(-1)}) = B$; *set* $n = -1$.

(1) *Solve for* $y^{(n+1)} = (u^{(n+1)}, \lambda^{(n+1)})^\top \in \mathbb{R}^N \times \mathbb{R}^{|B|}$:

$$Lu^{(n+1)} - \Lambda^\top \lambda^{(n+1)} = f, \tag{3.16a}$$

$$\begin{aligned} (\Lambda u^{(n+1)})_i &= 0 \quad \textit{for all } i \in A(y^{(n)}), \\ \lambda_i^{(n+1)} &= 0 \quad \textit{for all } i \in I(y^{(n)}). \end{aligned} \tag{3.16b}$$

(2) *Compute the active and inactive sets at* $y^{(n+1)}$:

$$A(y^{(n+1)}) = \{i \in B : \ c\lambda_i^{(n+1)} - (\Lambda u^{(n+1)})_i > 0\}, \tag{3.17a}$$

$$I(y^{(n+1)}) = \{i \in B : \ c\lambda_i^{(n+1)} - (\Lambda u^{(n+1)})_i \leq 0\}. \tag{3.17b}$$

(3) *If* $n \geq 0$ *and* $A(y^{(n+1)}) = A(y^{(n)})$ *then STOP; else set* $n = n+1$ *and go to step 1.*

Due to Step 2, which utilizes both the primal variable u and the dual variable λ, we shall refer to Algorithm 1 as the *primal-dual active set method*. It is equivalent to (3.15): In fact, we start by rewriting (3.15) as follows:

$$L(u^{(n+1)} - u^{(n)}) - \Lambda^\top(\lambda^{(n+1)} - \lambda^{(n)}) = f - Lu^{(n)} + \Lambda^\top\lambda^{(n)}, \tag{3.18a}$$

$$\begin{aligned} -\chi_{A(y^{(n)})}\Lambda(u^{(n+1)} - u^{(n)}) - c\chi_{I(y^{(n)})}(\lambda^{(n+1)} - \lambda^{(n)}) \\ = c\lambda^{(n)} - \max(c\lambda^{(n)} - \Lambda u^{(n)}, 0). \end{aligned} \tag{3.18b}$$

Equation (3.18a) implies (3.16a), and the non-smooth equation (3.18b) is realized by the choices (3.17) and (3.16b).

The stopping rule in Step 3 of Algorithm 1 is motivated by the following considerations. For $i \in A(y^{(n)})$ we have $(\Lambda u^{(n+1)})_i = 0$, and for $i \in I(y^{(n)})$ we obtain $\lambda_i^{(n+1)} = 0$. Hence, if we assume that $A(y^{(n)}) = A(y^{(n+1)})$, then from (3.17a) we infer $\lambda_i^{(n+1)} > 0$ for all $i \in A(y^{(n+1)})$, and $(\Lambda u^{(n+1)})_i \geq 0$ for all $i \in I(y^{(n+1)})$ by (3.17b). This, together with (3.16a), proves that the iterate $y^{(n+1)} = (u^{(n+1)}, \lambda^{(n+1)})^\top$ satisfies $F(y^{(n+1)}) = 0$ if Algorithm 1 terminates in Step 3. This actually occurs in all our numerical examples.

Based on Lemma 3.1, an application of the global convergence results given in [9, 10] leads to the following proposition.

Proposition 3.2. *Assume that $L = M + S$ with $M \in \mathbb{R}^{N\times N}$ a non-singular* M*-matrix and with $S \in \mathbb{R}^{N\times N}$ a perturbation such that $\|S\|_1$ is sufficiently small. Then:*

- **(i)** *Regardless of the initial choice, Algorithm 1 is well-defined, and the iterates $(u^{(n)}, \lambda^{(n)})^\top$ converge to the solution of* (3.3).
- **(ii)** *For the specific initialization of $\lambda^{(0)} = 0$ and $u^{(0)} = L^{-1}f$, the iterates $\Lambda u^{(n)}$ are feasible and they converge monotonically with $A(y^{(n-1)}) \supset A(y^{(n)})$ for $n \geq 1$.*

3.3. **Numerical example (continued).**

3.3.1. *Discretization.* We discretize problem (2.8) by finite elements. For the basis functions e^k related to the k-th nodal point of the triangulation, we order the displacement vector as

$$\ldots, (u_1)^k, (u_2)^k, (u_3)^k, \ldots, (u_1)^s, (u_2)^s, (u_3)^s, \ldots.$$

According to (2.6) the stiffness matrix L in (3.1) involves the following 3×3-cells:

$$\begin{bmatrix} C_{11}^\beta e_{,1}^k e_{,1}^s + C_{44}^\beta e_{,2}^k e_{,2}^s & C_{12}^\beta e_{,1}^k e_{,2}^s + C_{44}^\beta e_{,2}^k e_{,1}^s & C_{16}^\beta e_{,1}^k e_{,1}^s + C_{45}^\beta e_{,2}^k e_{,2}^s \\ C_{12}^\beta e_{,1}^k e_{,2}^s + C_{44}^\beta e_{,2}^k e_{,1}^s & C_{44}^\beta e_{,1}^k e_{,1}^s + C_{22}^\beta e_{,2}^k e_{,2}^s & C_{45}^\beta e_{,1}^k e_{,2}^s + C_{26}^\beta e_{,2}^k e_{,1}^s \\ C_{16}^\beta e_{,1}^k e_{,1}^s + C_{45}^\beta e_{,2}^k e_{,2}^s & C_{45}^\beta e_{,1}^k e_{,2}^s + C_{26}^\beta e_{,2}^k e_{,1}^s & C_{66}^\beta e_{,1}^k e_{,1}^s + C_{55}^\beta e_{,2}^k e_{,2}^s \end{bmatrix}$$

Following a common procedure in linear elasticity we utilize linear finite-elements on a triangular mesh constructed in Ω_C. For improved resolution of the singularity (crack tip), which may be located at any point along the interface, we use a local refinement in a neighborhood of Σ. This results in two mesh-parameters: h for the uniform mesh in the domain, and h_C for the fine mesh at the interface, as illustrated in Figure 4 for $h = 1/8$ and $h_C = h, h/2, h/4$.

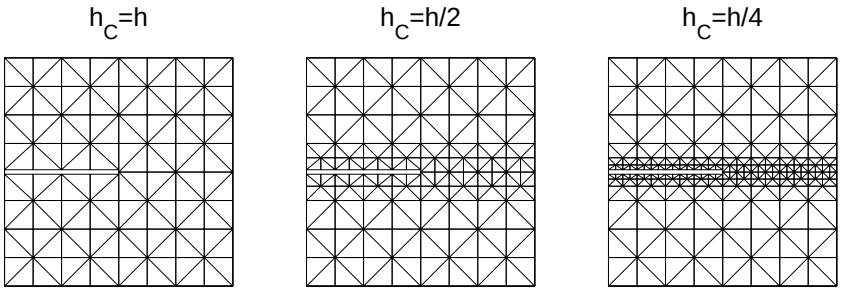

FIGURE 4. Adaptive meshing in Ω_C for $h = 1/8$.

Next we give the description of the matrix $\Lambda \in \mathbb{R}^{|B|\times N}$ in (3.1) with $B \subset \{1, \dots, N\}$. First let us define the index set $\mathcal{B} \subset B \times B$. Each pair $(i^+, i^-) \in \mathcal{B}$ corresponds to an index $i \in B$, which belongs to a nodal point at the crack Γ_C, *i.e.*, $i^+ = i^+(i)$ and $i^- = i^-(i)$. Thus, $|\mathcal{B}| = |B|$. This definition allows us to write the discrete non-penetration condition as

$$(u_2)^{i^+} - (u_2)^{i^-} \geq 0 \quad \text{for all } (i^+, i^-) \in \mathcal{B}, \tag{3.19}$$

where $u^{i^\pm} = ((u_1, u_2, u_3)^\top)^{i^\pm}$ are the displacement vectors at the nodal points on Γ_C^+ and Γ_C^-. Secondly, we assume that the vector $u \in \mathbb{R}^N$ is partitioned into $u = (u_D, u_{\tilde{B}})^\top$ with the index set $\tilde{B}$ and the vector $u_{\tilde{B}}$ defined as follows: Let $u_2^{B^+} = ((u_2)^{i^+(1)}, \dots, (u_2)^{i^+(B)}) \in \mathbb{R}^{|B|}$, and analogously for $u_2^{B^-}$. Then $u_{\tilde{B}} = (u_2^{B^+}, u_2^{B^-})^\top \in \mathbb{R}^{2|B|}$. Thus, we infer that $|\tilde{B}| = 2|B|$. Now, the matrix Λ can be expressed as

$$\Lambda = (\mathbf{0}, \chi_{u_2^{B^+}}, -\chi_{u_2^{B^-}}),$$

where $\mathbf{0}$ is the $|B| \times |D|$-zero matrix with $|D| = N - |\tilde{B}|$. The column-rank of Λ is $|B|$. Therefore, Λ is related to the discretized non-penetration condition (3.19).

3.3.2. *Implementation of the primal-dual active-set algorithm.* We consider the example of Section 2.4. As we shall see the primal-dual active set algorithm possesses the properties stated in Proposition 3.2.

We decompose the stiffness matrix L as $L = M + S$ with M an M-matrix and S a perturbation. In relation to Proposition 3.2, the 1-norms of L, M, and S are presented in Figure 5 for a typical value of h and $h/h_C = 4$ for β chosen in $[0, \pi/2]$. These results are rather independent of h. For the remainder of this section we fix $\beta = \pi/8$.

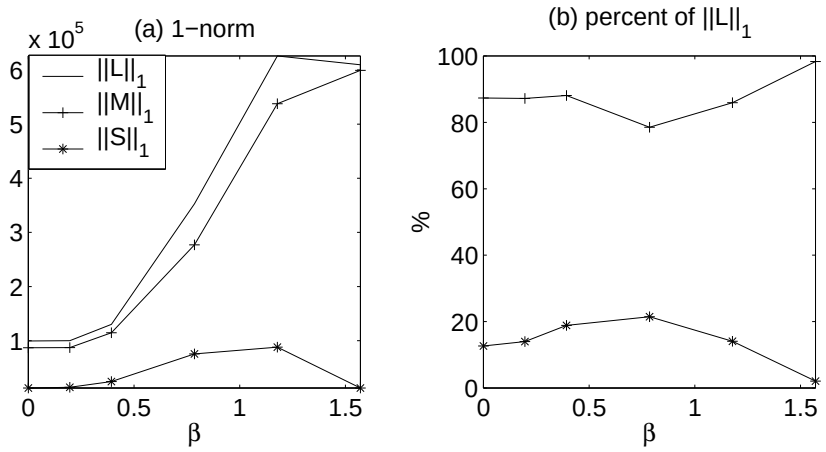

FIGURE 5. Decomposition of the stiffness matrix L.

In all cases tested, Algorithm 1 terminated after finitely many iterates by producing the same active/ inactive set structure in two consecutive iterations. Thus it found the exact solution of the discretized problem (3.1). For $l = 0.5$ the number of iterations required for the successful termination of the algorithm is presented in Table 1 for various mesh-sizes h and h_C. Table 1 shows that the number of iterations (#it) is rather small and increases moderately when the mesh is refined. We utilized the specific initialization $A(y^{(-1)}) = \emptyset$, $I(y^{(-1)}) = B$,

#it/ $h_C =$	1/20	1/40	1/80	1/160	1/320	1/640	1/1280
$h = 1/20$	3	4	5	6	6	-	-
$h = 1/40$	-	4	4	5	7	7	-
$h = 1/80$	-	-	5	5	7	9	9

TABLE 1. Number of iterations for fixed grid method.

which corresponds to

$$\lambda^{(0)} = 0, \quad u^{(0)} = L^{-1} f \tag{3.20}$$

in (3.15). We choose c of the order 10^{-8} in the definition of the active and inactive sets in (3.17).

Concerning the monotonicity properties of the Newton iterates, we next present the primal variable $\Lambda u = [\![u_2]\!]$ in (3.19), the dual variable $\lambda = -\sigma_{22}(u)$ according to (2.17), and the characteristic function $\chi_{A(y)}$ of the active set $A(y)$ at the interface Σ, respectively. First let $l = 0.75$, $h = 1/40$, and $h_C = 1/160$. The iterates $\Lambda u^{(n)}$ and $\lambda^{(n)}$ are depicted in Figure 6 (a) and (b), respectively, for $n = 0, \ldots, 8$. The results

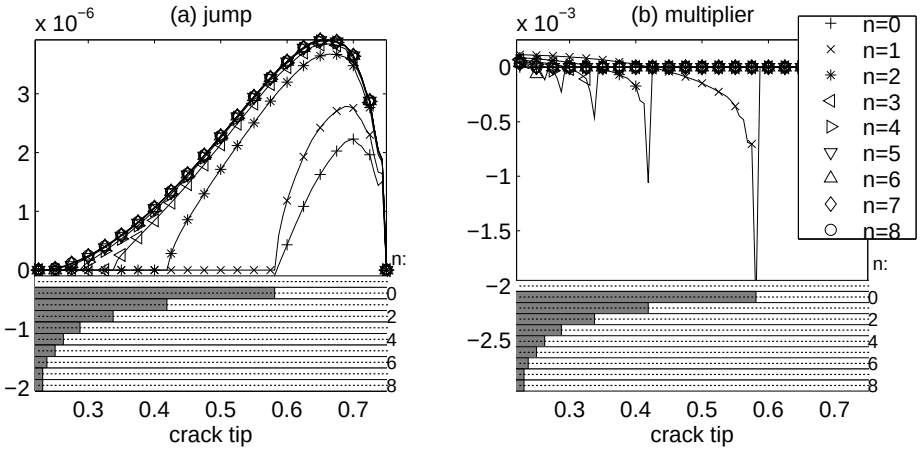

FIGURE 6. Iterates $\Lambda u^{(n)}$, $\lambda^{(n)}$, and $A(y^{(n)})$ for $l = 0.75$.

are provided only for the interval $x_1 \in [0.22, 0.75]$ near the crack tip where the active/ inactive structure is changing. On $x_1 \in [0, 0.22)$ the solution is active for all $n \geq 0$. For convenience the characteristic function of the active sets $A(y^{(n)})$ for $n = -1, 0, \ldots, 8$ is indicated below the graphs. We observe from Figure 6 a monotonic behavior of $\Lambda u^{(n)} \geq 0$ and $A(y^{(n-1)})$, but not of $\lambda^{(n)}$. Note further that from one iteration to the next several grid points are removed from the active set.

The results for another set of data with $l = 0.5$, $h = 1/40$ and $h_C = 1/640$ are presented in Figure 7 in the interval $[0.42, 0.5]$. The remaining interval $x_1 \in [0, 0.42)$ is split into two subsets: an active and an inactive one near $x_1 = 0$. In Figure 7 we see also that the active set splits locally near the crack tip into separate intervals. At iteration $n = 6$ the algorithm stops with 2 active and 3 inactive subintervals.

From all examples tested we can report the following properties of the Newton iterates according to Algorithm 1: the iterates are feasible, *i.e.*, $\Lambda u^{(n)} \geq 0$, and they converge monotonically $\Lambda u^{(n)} \geq \Lambda u^{(n-1)}$ with $A(y^{(n-1)}) \supset A(y^{(n)})$ for $n \geq 1$. This is in accordance with the assertion of Proposition 3.2.

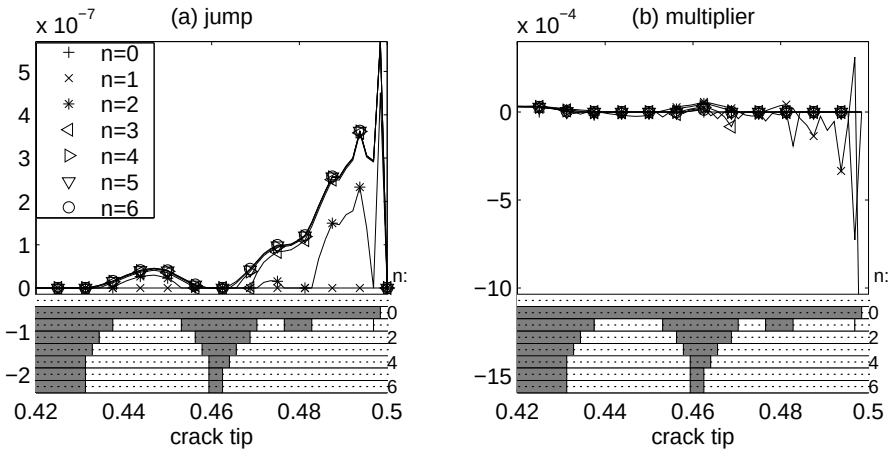

FIGURE 7. Iterates $\Lambda u^{(n)}$, $\lambda^{(n)}$, and $A(y^{(n)})$ for $l = 0.5$.

For a reduction of the computational costs, we also used a continuation technique: We solved (3.15) with (3.20) on a coarse grid with $h_C = h$, and subsequently used prolongation of this solution and its corresponding multiplier as initial values on increasingly finer meshes with mesh-size $h_C < h$, respectively. For $l = 0.75$, in Table 2 the

#it	$h_C =$	1/20	1/40	1/80	1/160	1/320	1/640	1/1280
$h = 1/20$	fixed	5	7	8	9	9	-	-
$h = 1/20$	cont.	5	+2	+2	+2	+2	-	-
$h = 1/40$	fixed	-	7	8	9	10	12	-
$h = 1/40$	cont.	-	7	+2	+2	+2	+2	-
$h = 1/80$	fixed	-	-	8	9	10	11	12
$h = 1/80$	cont.	-	-	8	+2	+1	+2	+2

TABLE 2. Number of iterations for fixed grid and the continuation method.

first row shows the number of iterations required by Algorithm 1 for a fixed grid. The second row presents the results for the continuation technique. The entry '+2' (or '+1') indicates that only two (or one) iterates are required on the next finer grid for a successful termination with $A(y^{(1)}) = A(y^{(0)})$ (or $A(y^{(0)}) = A(y^{(-1)})$). These results show that the continuation technique is an effective tool for reducing costly fine grid iterations.

3.3.3. *Mesh refinement.* In this section we consider the results as h and h_C are decreased. For $l = 0.75$ the jump Λu and the corresponding multiplier λ obtained by Algorithm 1 are depicted in Figure 8 (a) and (b). Representative results for $h = 1/40$ with $h_C = 1/40$ and

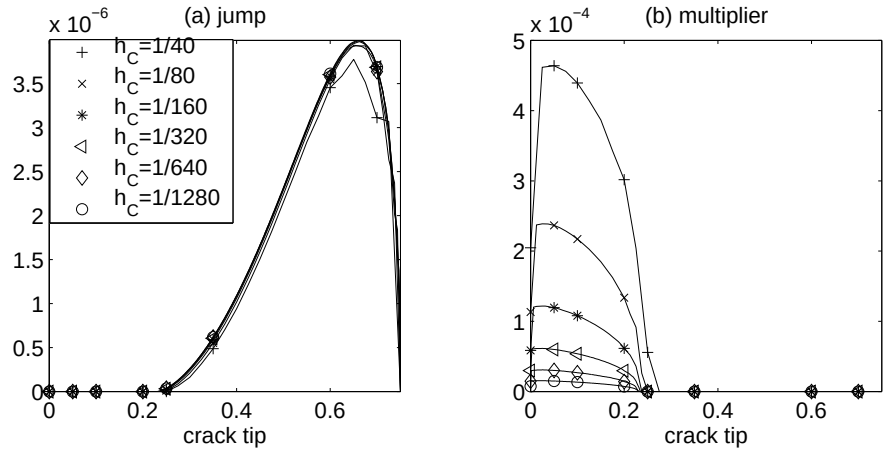

FIGURE 8. Solutions Λu and λ for $l = 0.75$.

$h_C = 1/640$, and for $h = 1/80$ with $h_C = 1/80, 1/160, 1/320, 1/1280$ are shown. We see that the solutions Λu are visually almost undistinguishable if $h_C \leq 1/80$, and that λ converges monotonically as h_C decreases. The characteristic functions of the corresponding active sets are illustrated in Figure 9 (a). Monotone convergence of $A(y)$ can be observed if both mesh-size parameters decrease.

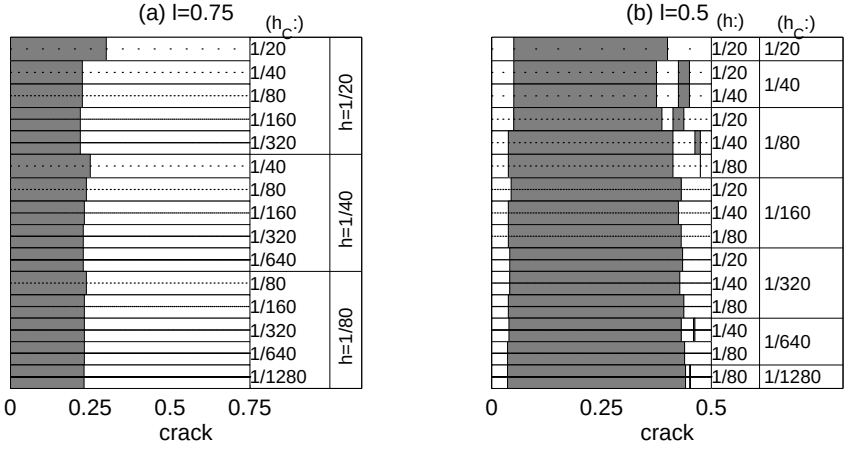

FIGURE 9. History of active sets $A(y)$.

This is not the case for the crack problem with $l = 0.5$ illustrated in Figure 9 (b). We observe a monotonous behavior near the edge $x_1 = 0$, and a flattering of the active set near the crack tip $x_1 = 0.5$. This behavior persists even when we increase the accuracy `tol` for the iterative solver for the linear system in Step 1 of Algorithm 1. Typically the outer iteration terminates due to coincidence of two successive iterations. The solutions Λu and λ in the neighborhood of the crack tip at $[0.42, 0.5]$ are depicted in Figure 10 (a) and (b) for $\texttt{tol} \in [10^{-14}, 10^{-8}]$, with the same values for (h_C, h) as stated above. In Figure 10, again

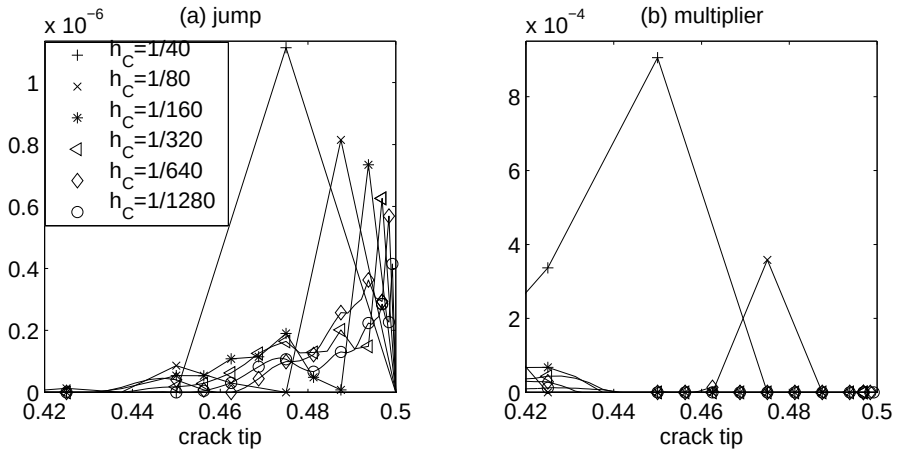

FIGURE 10. Solutions Λu and λ for $l = 0.5$.

we see a flattering of the jump $[\![u_2]\!]$ between the corresponding active/ inactive intervals. However, we shall see that the solution u itself converges linearly in the energy norm.

To interpret the flattering effect, let us note that the active set and the crack tip are geometrically separated from each other in the case $l = 0.75$. For $l = 0.5$, however, two geometrical singularities occur simultaneously in a neighborhood of the crack tip: one is connected to the non-penetration conditions resulting in the active set, and the other one is due to the transmission conditions imposed at the joint part of the interface. The phenomenon of flattering means that in the limit case ($h \to 0$), which corresponds to the continuous problem, it may happen that there is not only one, but possibly several points (finitely or infinitely many) separating the active/ inactive sets which are accumulating in a neighborhood of the crack tip. Alternatively, there may exist a non-zero interval where both the primal and the dual components of the solution are zero, *i.e.*, $[\![u_2]\!] = \sigma_{22}(u) = 0$, (see [25] for an account of oscillations at an interfacial crack).

4. Delamination of the composite via global shape optimization

Based on the model introduced in Section 2, we are now interested in the quasi-static delamination of the composite with a crack. This leads to a time-evolution problem for the (global) shape optimization of the total potential energy with respect to the crack length. For its numerical realization we rely on the algorithm analyzed in Section 3.

It was observed in experiments [15] that the assumption of crack propagation along a predefined path is physically consistent for laminar materials. To describe the delamination between Ω^+ and Ω^- in our model, we fix the length l_0 of an initial crack at $t = 0$ and look for its "time"-evolution $l(t) \geq l_0$ with respect to a (loading) parameter $t > 0$. With one crack tip fixed, the length-parameter $l(t)$ determines the position of the second crack tip at $t \geq 0$.

In a natural way we arrive at a one-parameter shape optimization problem. At every time-step t, the global setting consists of the minimization of an *a priori* given cost functional $T(l)$ (the total potential energy) over all admissible crack lengths $l \geq l_0$. This formulation requires to solve (2.12) with the crack Γ_C of length l to obtain $T(l)$. Employing the shape derivative of the cost function at l_0 provides the local optimality condition, which coincides with the Griffith fracture criterion. We combine these two approaches to derive a computationally constructive strategy for shape optimization.

4.1. Reduced potential energy function and its shape derivative.

For $L > 0$ let the crack Γ_C at the interface $\Sigma = \{0 \leq x_1 \leq L, x_2 = 0\}$ be given by the set

$$\Gamma_C = \{0 < x_1 < l, \quad x_2 = 0\}, \quad 0 \leq l \leq L. \tag{4.1}$$

Specifically we assume that the left crack-tip $(0,0)^\top$ is fixed on the boundary $\partial\Omega$ and the right tip $(l,0)^\top$ is located at the interface inside Ω. If $l = L$ then the right end of the crack meets $\partial\Omega$.

For the crack (4.1) a reduced potential energy function P depending on the crack-length parameter $l \in [0, L]$ is defined according to (2.10) and (2.12):

$$P(l) := \Pi(u) = \min_{v \in K(\Omega_C)} \Pi(v). \tag{4.2}$$

From (4.2) we deduce that P is a continuous, decreasing, and uniformly bounded function:

$$P \in C([0, L]), \quad 0 \geq P(\bar{l}) \geq P(l) \geq P(L) \text{ for } 0 \leq \bar{l} \leq l \leq L. \tag{4.3}$$

Fix $l \in (0, L)$ and let B_0, B_1 be such that $(l, 0)^\top \in B_1 \subset B_0 \subset \Omega$. Let $\chi \in W^{1,\infty}(\mathbb{R}^2)$ be an arbitrary cut-off function with support in a neighborhood of the crack tip, such that $\chi = 1$ in B_1 and $\chi = 0$ outside of B_0. For the solution u of (2.12), the shape derivative $P'(l)$ of (4.2) (in direction $(\chi, 0)^\top$) is found to be (see [16]):

$$P'(l) = \int_{\Omega_C} \sigma_{ij}(u)\big(\frac{1}{2}\chi_{,1}\varepsilon_{ij}(u) - E_{ij}(\nabla\chi; u)\big)\, dx, \tag{4.4}$$

where E denotes a 3×3-symmetric tensor (with $E_{33} = 0$) of the generalized strain

$$\begin{aligned} &E_{11}(\nabla\chi; u) = \chi_{,1}u_{1,1}, \quad E_{22}(\nabla\chi; u) = \chi_{,2}u_{2,1}, \\ &E_{12}(\nabla\chi; u) = 0.5(\chi_{,2}u_{1,1} + \chi_{,1}u_{2,1}), \\ &E_{23}(\nabla\chi; u) = 0.5\chi_{,2}u_{3,1}, \quad E_{13}(\nabla\chi; u) = 0.5\chi_{,1}u_{3,1}. \end{aligned} \tag{4.5}$$

In view of (2.6) and (2.7) we can express the integrand of (4.4) in $\Omega_C^\pm$ as the following quadratic form, which is neither positive nor negative definite (compare with (2.11)):

$$\begin{aligned} &-\frac{1}{2}C_{11}^\beta\chi_{,1}(u_{1,1}^\pm)^2 + C_{22}\big(\frac{1}{2}\chi_{,1} - \chi_{,2}\big)(u_{2,2}^\pm)^2 - C_{12}^\beta\chi_{,2}u_{1,1}^\pm u_{2,2}^\pm \\ &\mp C_{16}^\beta\chi_{,1}u_{1,1}^\pm u_{3,1}^\pm \mp C_{26}^\beta\chi_{,2}u_{2,2}^\pm u_{3,1}^\pm + \frac{1}{2}C_{55}^\beta\chi_{,1}(u_{3,2}^\pm)^2 - \frac{1}{2}C_{66}^\beta\chi_{,1}(u_{3,1}^\pm)^2 \\ &-\chi_{,2}(C_{44}^\beta u_{1,1} \pm C_{45}^\beta u_{3,1}^\pm)(u_{1,2}^\pm + u_{2,1}^\pm) + \frac{1}{2}C_{44}^\beta\chi_{,1}\big((u_{1,2}^\pm)^2 - (u_{2,1}^\pm)^2\big) \\ &\pm C_{45}^\beta(\chi_{,1}u_{1,2}^\pm - \chi_{,2}u_{1,1}^\pm)u_{3,2}^\pm - C_{55}^\beta\chi_{,2}u_{3,1}^\pm u_{3,2}^\pm. \end{aligned}$$

The value of $-P'(l)$ describes the energy release rate at the vicinity of the crack and is independent of χ. In fact, let us integrate by parts (4.4) in $\Omega_C \setminus B_1$, using (2.8) and $\chi = 1$ in B_1. For an outward normal vector $b = (b_1, b_2)^\top$ at ∂B_1, an equivalent representation of the shape derivative by the integral over a closed contour ∂B_1 (see [16]) is obtained:

$$P'(l) = \int_{\partial B_1} \sigma_{ij}(u)\big(\frac{1}{2}b_1\varepsilon_{ij}(u) - E_{ij}(b; u)\big)\, ds \tag{4.6}$$

with b_1 and b_2 replacing $\chi_{,1}$ and $\chi_{,2}$ in (4.5). For $\beta = 0$ and $u_3 = const$ formula (4.6) coincides with the path-independent Cherepanov-Rice integral, which is well-known in fracture mechanics.

From (4.4) and (4.3) we can conclude that

$$P' \in C(0, L), \quad P'(l) \le 0. \tag{4.7}$$

Let us notice the general fact that for unilaterally constrained crack problems the second derivatives P'' is set-valued.

4.2. **Evolutionary problem for shape optimization.** We assume that the loading depends in a linear way on a parameter $t \geq 0$:

$$g(t) = tg. \tag{4.8}$$

In view of the multiplicative property of the static problem (2.13) it follows that $u(t) = tu$ is a solution of the quasi-static problem: Find $u(t) \in K(\Omega_C)$ such that

$$\int_{\Omega_C} \sigma_{ij}(u(t))\varepsilon_{ij}(v - u(t))\,dx \geq t \int_{\Gamma_N} g_i(v - u(t))_i\,ds \quad \text{for all } v \in K(\Omega_C). \tag{4.9}$$

We arrive at the reduced potential energy function which is quadratic in t:

$$P(l)(t) = t^2 P(l), \quad P'(l)(t) = t^2 P'(l). \tag{4.10}$$

In addition to the potential energy let us introduce the surface energy at the crack faces $\Gamma_C^{\pm}$,

$$S(l) := \Big(\int_{\Gamma_C^+} + \int_{\Gamma_C^-}\Big)\frac{1}{2}\gamma\,ds = \gamma\,l, \tag{4.11}$$

where the physical parameter γ is a given constant and expresses twice the density of the surface energy distributed uniformly at the crack. The total potential energy T is defined as the sum of P from (4.10) and S from (4.11):

$$T(l)(t) := P(l)(t) + S(l) = t^2 P(l) + \gamma l. \tag{4.12}$$

Let an initial crack with $l_0 \in (0, L)$ be fixed at $t = 0$. To determine an actual state $l(t)$ of the crack for $t > 0$ following the principle of virtual work, we have to minimize the total potential energy over all admissible cracks. The standard assumption of brittle fracture does not allow the crack to disappear. In this way, from (4.12) we arrive at a shape optimization problem at every "time" t subject to a constraint $l \geq l_0$:

$$\text{minimize } \gamma l + t^2 P(l) \quad \text{over } l \in [l_0, L]. \tag{4.13}$$

Due to the linearity of $S(l)$ and (4.3), the function $T(l)$ is bounded and uniformly continuous in $[0, L]$. Hence there exists a global minimizer $l(t) \in [l_0, L]$ for (4.13) satisfying

$$\gamma l(t) + t^2 P(l(t)) \leq \gamma l + t^2 P(l) \quad \text{for all } l \in [l_0, L], \quad t \geq 0. \tag{4.14}$$

It can be verified (see [5]) that the necessary and sufficient conditions for (4.14) are given by the system:

$$l(0) = l_0, \tag{4.15a}$$

$$l(t) \geq l(s) \quad \text{for } t > s, \tag{4.15b}$$

$$\gamma l(t) + t^2 P(l(t)) \leq \gamma l + t^2 P(l) \quad \text{for all } l \geq l^-(t), \tag{4.15c}$$

$$\gamma l(t) + t^2 P(l(t)) \leq \gamma l(s) + t^2 P(l(s)) \quad \text{for all } s \leq t. \tag{4.15d}$$

Here, we use the notation $l^-(t) = \lim_{s \to t} l(s)$ for $s < t$, and analogously $l^+(t) = \lim_{s \to t} l(s)$ for $s > t$. In fact, the initial condition at $t = 0$ implies (4.15a), the model of brittle fracture requires that $l(t)$ should be an increasing function of t as written in (4.15b), and (4.15c)–(4.15d) follow directly from (4.14). In view of (4.7), the differentiability of P and (4.15c) lead to the necessary optimality condition

$$\gamma + t^2 P'(l(t)) \geq 0. \tag{4.16}$$

It is important to note that (4.15d) holds true in the case where l is continuous as well as in the case of a jump $l^+(t) \neq l^-(t)$. The jump can be characterized by

$$\gamma[l^+(t) - l^-(t)] + t^2[P(l^+(t)) - P(l^-(t))] = 0. \tag{4.17}$$

Alternatively, if $l(t)$ were a uniformly continuous function, then $l^+(t) = l^-(t)$ in (4.17) and the Griffith law of fracture would be satisfied:

$$\begin{aligned} &l(0) = l_0, \\ &l'(t) \geq 0,\ \gamma + t^2 P'(l(t)) \geq 0,\ l'(t)\big(\gamma + t^2 P'(l(t))\big) = 0, \quad t \geq 0. \end{aligned} \tag{4.18}$$

The set of critical points for (4.13) is given by:

$$M_t = \begin{cases} L, \\ l_0 \quad \text{if } \gamma + t^2 P'(l_0) \geq 0, \\ l \quad \text{if } \gamma + t^2 P'(l) = 0 \quad \text{and } l \geq l(s) \text{ for } s \leq t. \end{cases} \tag{4.19}$$

Using non-positivity of P' we define

$$G(t, l) := t - \sqrt{\gamma/(-P'(l))}, \quad P'(l) \neq 0 \tag{4.20}$$

and rewrite (4.19) as

$$M_t = \begin{cases} L, \\ l_0 \quad \text{if } G(t, l_0) \leq 0 \quad \text{or } P'(l_0) = 0, \\ l \quad \text{if } G(t, l) = 0 \quad \text{and } l \geq l(s) \text{ for } s \leq t. \end{cases} \tag{4.21}$$

Further, (4.13) is equivalent to

$$
\begin{aligned}
&l(0) = l_0,\\
&\text{minimize } \gamma l + t^2 P(l) \quad \text{over } l \in M_t \quad \text{for } t > 0.
\end{aligned}
\tag{4.22}
$$

The advantage of our formulation (4.22) is related to the fact that it not only uses function values $T(l)$ but also the derivatives $T'(l)$ which gives a more accurate account of the extrema. In the numerical realization we find that for (4.13) a finer discretization with respect to l is necessary to achieve the same accuracy as (4.22).

4.3. **Numerical example (continued).**

4.3.1. *The discrete potential energy and its derivative.* In this and the following section we consider the example of Section 2.4 with a mode-3 surface traction. For $l \in [0, 1]$ the numerical solution of (3.1) is computed by the algorithm described in Section 3 . The reduced potential energy function P and its shape derivative are obtained from (2.10) and (4.4). For numerical calculations the cut-off function χ in formula (4.4) is taken piecewise-linear in Ω with $\chi = 1$ around the crack tip, $\chi = 0$ near the external boundary $\partial\Omega$, and symmetrically centered with respect to each crack tip. For $l = 0.5$ and $\beta = \pi/8$ the numerical values of P and P' are depicted for various mesh-sizes h and h_C in Figure 11. These graphs show linear dependence of both P and P' on h as well as

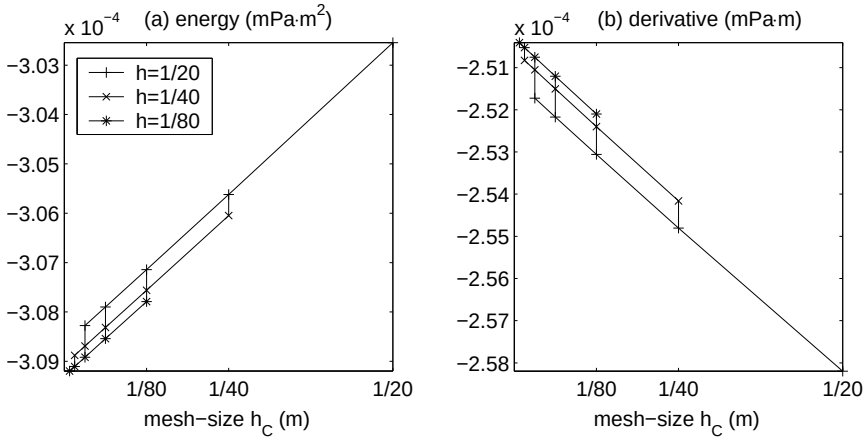

FIGURE 11. Error of the discretization.

h_C. In further calculations we fix the mesh-parameters $h = 1/80$ and $h_C = 1/320$.

We approximate the functions P and P' by its discrete values in nodal points $l = 0, h, \ldots, 1$, respectively $l = h, 2h, \ldots, 1 - h$ for $P'(l)$.

The results are depicted in Figure 12 for various fibering angles $\beta = 0, \pi/16, \pi/8, \pi/4, 3\pi/8, \pi/2$. Here mPa stands for mega Pascal. We

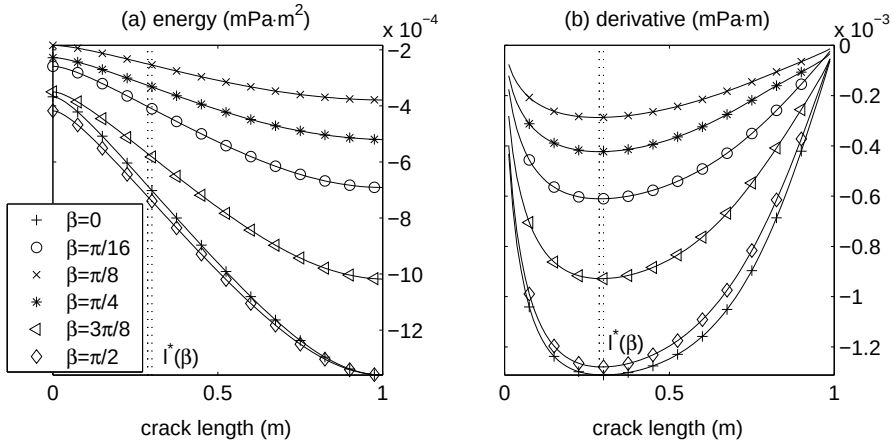

FIGURE 12. Potential energy and its shape derivative.

find regions of convexity and concavity of P and minima of $P'(l)$:

$$P'(l^\star) \le P'(l) \quad \text{for all } l, \tag{4.23}$$

which occur for $l^\star \approx 0.3$ if $\beta \in \{0, \pi/2\}$, and for $l^\star \approx 0.2875$ if $\beta \in \{\pi/16, \pi/8, \pi/4, 3\pi/8\}$. They are marked by dotted-lines in the figure.

From Figure 12 we observe the following properties:

- $P(l) < 0$, $P'(l) < 0$ for all β, the limit cases $\beta = 0$ and $\beta = \pi/2$ are close to each other.
- $\beta \to P$ and $\beta \to P'$ increase for $\beta \in [0, \pi/8]$ and decrease for $\beta \in [\pi/8, \pi/2]$.
- $P(l)$ is concave on $(0, l^\star)$ and convex on $(l^\star, 1)$ for all β.

4.3.2. *Delamination under mode-3 loading.* Now we apply the numerical data from Figure 12 and describe a quasi-static delamination of the composite with crack. For numerical tests the physical parameter γ is taken as $\gamma = 25^2/2\mu \approx 0.011$ (mPa·m).

To endow the loading parameter $t \ge 0$ with a physical scale we multiply it by g_0 and consider the linear loading $g_0 t$ (mPa) according to (4.8). Since $P'(l)$ is negative $G(t, l)$ in (4.20) is well-defined and $g_0 t(l)$ can be obtained from

$$0 = g_0 G(t, l) = g_0 t - g_0 \sqrt{\gamma/(-P'(l))}. \tag{4.24}$$

For $\beta = \pi/8$ this curve is shown in Figure 13 (a) and (b), respectively, by a dashed-line. In the remainder of this section we analyze the function T defined in (4.12) with respect to local and global minima using

(4.18) and (4.22), respectively. The curve defined in (4.24) contains all critical points of T inside the optimization interval.

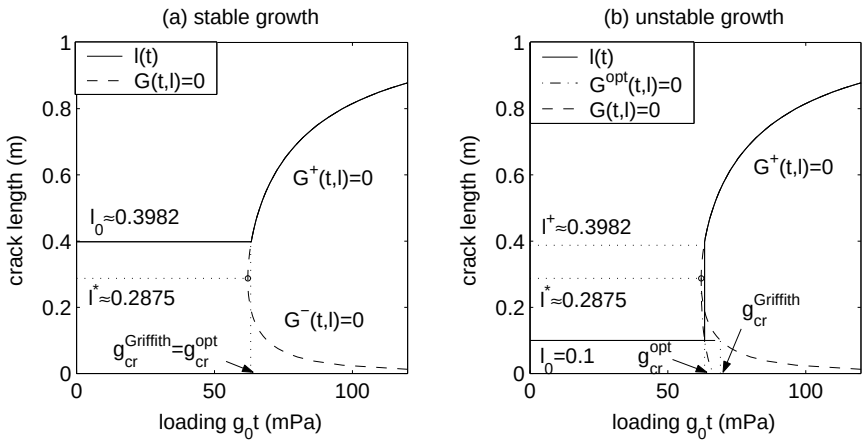

FIGURE 13. Quasi-static crack growth as $\beta = \pi/8$.

We start with the discussion of local minima and fix an arbitrary $l_0 \in (0,1)$. Following the Griffith fracture hypothesis, a critical loading required to start the growth of a crack of length l_0 is determined from (4.24) by

$$g_{\rm cr}^{\rm Griffith}(l_0) := g_0 t(l_0) \quad \text{where } G(t(l_0), l_0) = 0. \tag{4.25}$$

Then the constant function $l(t) = l_0$ is the unique solution to (4.18) as long as $G(t, l_0) < 0$.

Next we seek for the solution $l(t)$ to (4.18) for t such that $G(t, l_0) \geq 0$. For this purpose points $l^\star \in (0,1)$ of local extrema of $t(l)$ must be found. For our data we obtain one minimizer $l^\star$ which is equivalently characterized by

$$G(t, l^\star) \geq G(t, l) \quad \text{for all } l, \tag{4.26}$$

independently of t. For $\beta = \pi/8$ we obtain $l^\star \approx 0.2875$, which is marked with a dotted-line in Figure 13. The line $l = l^\star$ separates $G(t,l) = 0$ into two branches along which $l(t)$ is invertible. These two branches are given by $G^-(t,l) = 0$ for $l \in (0, l^\star)$, and $G^+(t,l) = 0$ for $l \in [l^\star, 1)$. The local solution $l(t) = l_0$ of (4.18) meets either $G^-(t,l) = 0$ if $l_0 < l^\star$, or $G^+(t,l) = 0$ if $l_0 \geq l^\star$. In the latter case $l(t)$ is an increasing function. Therefore if $l_0 \in [l^\star, 1)$, then $l(t)$ satisfying $G^+(t, l(t)) = 0$ is the unique continuous solution to (4.18) for all t. Alternatively, $l(t)$ obtained from $G^-(t,l) = 0$ is a decreasing function. Hence if $l_0 \in (0, l^\star)$ then there

is no solution $l(t)$ to (4.18), which is continuous at the points $t(l_0)$ satisfying $G(t, l_0) = 0$.

To explain the non-existence of a solution to (4.18) we observe that this relation constitutes a local optimality criterion for (4.13). In our example this results in the following: The points $l^\star$ found by (4.23) and (4.26) coincide. Thus $P(l)$ (and hence the total energy $\gamma l + t^2 P(l)$) is convex along the branch $G^+(t, l) = 0$ and concave along $G^-(t, l) = 0$. Hence, points $l(t)$ located on $G^+(t, l) = 0$ provide minima of the total potential energy, whereas points on $G^-(t, l) = 0$ give its local maxima.

Now we look for a global minimizer of the shape optimization problem (4.14) represented in the form (4.22). Solving it numerically we find continuous solutions for initial cracks of the length $l_0 \in [l^\star, 1)$, which coincide with those obtained by the Griffith fracture law (4.18). For $\beta = \pi/8$ and $l_0 \approx 0.3982$ the solution $l(t)$ to (4.21), (4.22) is depicted in Figure 13 (a) with a solid-line. For initial cracks of the length $l_0 \in (0, l^\star)$ we derive discontinuous solutions with a jump $l^+ - l_0 > 0$ at the point t where the jump condition (4.17) is satisfied, *i.e.*

$$
\begin{aligned}
&g_{\rm cr}^{\rm opt}(l_0) := g_0 t \text{ where } t \text{ satisfies} \\
&G(t, l^+) = 0, \quad \text{and} \quad \gamma[l^+ - l_0] + t^2[P(l^+) - P(l_0)] = 0.
\end{aligned} \tag{4.27}
$$

For $\beta = \pi/8$ and $l_0 = 0.1$ the solution $l(t)$ to (4.21), (4.22) is depicted in Figure 13 (b) with a solid-line. We find numerically that $l^+ \approx 0.3982$ (this value for l_0 was chosen in the previous example of stable propagation), $g_{\rm cr}^{\rm opt} \approx 63$ (mPa) and $g_{\rm cr}^{\rm Griffith} \approx 69$ (mPa). Here the value of critical loading obtained by the shape optimization approach from (4.27) is smaller than the one predicted by the Griffith fracture criterion (4.25).

We obtain an improved curve of critical loading by determining $t(l)$ from the following equation

$$
0 = G^{\rm opt}(t, l) := \begin{cases} G^+(t, l) & \text{for } l \in [l^\star, 1), \\ g_0 t - g_{\rm cr}^{\rm opt}(l) & \text{for } l \in (0, l^\star), \end{cases} \tag{4.28}
$$

where $g_{\rm cr}^{\rm opt}(l)$ is computed according to (4.27) using (4.22) and (4.21) for all discrete length-parameters $l \in (0, l^\star)$. For $\beta = \pi/8$ this curve is depicted in Figure 13 (b) with a dash-dotted line.

The delamination of the composite with the initial crack of length $l_0 \in (0, 1)$ under linear quasi-static loading $g_0 t$ can be constructed geometrically by the following algorithm.

Algorithm 2.

(0) *Fix the initial crack length* $l_0 \in (0, 1)$, *find* $t(l_0)$ *such that* $G^{\rm opt}(t(l_0), l_0) = 0$.

(1) *For all* $t < t(l_0)$ *we have* $l(t) = l_0$ *(no growth).*
(2) *At* $t = t(l_0)$ *find* $l(t) = \max\{l_0, l^+\}$*, such that* l^+ *satisfies* $G^{\rm opt}(t(l_0), l^+) = 0$ *(initiation of crack growth).*
(3) *For all* $t > t(l_0)$ *find* $l(t)$ *such that* $G^+(t, l(t)) = 0$ *(crack growth).*

If $l^+ = l_0$ in Step 2 then the propagating crack is stable and it grows in a continuous way. Otherwise, if $l^+ > l_0$ then the crack propagation is unstable with the jump $l^+ - l_0$.

Next we solve $G^{\rm opt}(t, l) = 0$ for various choices for the fibering angle $\beta = 0, \pi/16, \pi/8, \pi/4, 3\pi/8, \pi/2$. The results are depicted in Figure 14, and are compared to the solutions of $G(t, l) = 0$ according to the Griffith law (4.25) indicated by dashed lines. The points $l^\star(\beta)$ separating

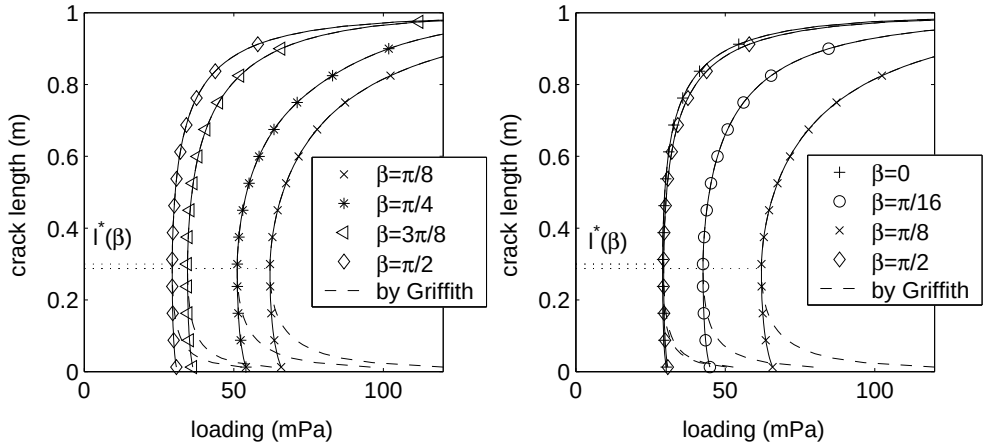

FIGURE 14. Curves $G^{\rm opt}(t, l) = 0$ of critical loading.

the intervals of stable and unstable crack propagation are indicated by dotted-lines. For every initial crack of length l_0 the delamination process can be constructed by Algorithm 2.

From Figure 14 we can report on the following features:

- The toughness with respect to the critical mode-3 loading of the composite materials is maximal at $\beta = \pi/8$.
- The curves for the limit cases $\beta = 0$ and $\beta = \pi/2$ are close to each other.
- In the interval $[l^\star, 1)$ the crack growth is stable, otherwise it is unstable.

Figure 14 shows clearly that $g_{\rm cr}^{\rm Griffith}(l_0) \to \infty$ as $l_0 \to 0$. To explain this behavior, note that the limit case $l_0 = 0$ corresponds to

the initialization of a crack in a continuous solid which can not be described exactly by the above macro-crack model. Nevertheless, from Figure 14 we may conjecture that $g_{\rm cr}^{\rm opt}(0) < \infty$, which is more consistent physically than $g_{\rm cr}^{\rm Griffith}(0) = \infty$. The other limit behavior $g_{\rm cr}^{\rm opt}(l_0) = g_{\rm cr}^{\rm Griffith}(l_0) \to \infty$ as $l_0 \to 1$ is due to the boundary condition describing a clamped edge at $l = 1$.

Acknowledgment. The research results were obtained with the support of the Austrian Science Fund (FWF) in the framework of the SFB project F003 "Optimierung und Kontrolle", and the Russian Foundation for Basic Research (03-01-00124).

References

[1] M. Bach, S.A. Nazarov and W.L. Wendland, Stable propagation of a mode-1 planar crack in an anisotropic elastic space. Comparison of the Irwin and the Griffith approaches, *Current Problems Anal. Math. Phys. (Taormina, 1998)*, 167–189, Aracne, Rome, 2000.

[2] E.G. Cherepanov, *Mechanics of Brittle Fracture*, McGrow-Hill, 1979.

[3] R. Cottle, J.-S. Pang and R.E. Stone, *The Linear Complementarity Problem*, Academic Press, Boston, 1992.

[4] G. Dal Maso and R. Toader, A model for the quasistatic growth of brittle fractures: Existence and approximation results, *Arch. Rational Mech. Anal.* **162** (2002), 101–135.

[5] G.A. Francfort and J.-J. Marigo, Revisiting brittle fracture as an energy minimization problem, *J. Mech. Phys. Solids* **46** (1998), 1319–1342.

[6] A. Friedman and Y. Liu, Propagation of cracks in elastic media, *Arch. Rat. Mech. Anal.* **136** (1996), 235–290.

[7] M. Hintermüller, K. Ito and K. Kunisch, The primal-dual active set strategy as a semismooth Newton method, *SIAM J. Optim.* **13** (2003), 865–888.

[8] M. Hintermüller, V.A. Kovtunenko and K. Kunisch, The primal-dual active set method for a crack problem with non-penetration, *IMA J. Appl. Math.* **69** (2004), 1–26.

[9] M. Hintermüller, V.A. Kovtunenko and K. Kunisch, Semismooth Newton methods for a class of unilaterally constrained variational problems, *Adv. Math. Sci. Appl.*, to appear.

[10] M. Hintermüller, V.A. Kovtunenko and K. Kunisch, Generalized Newton methods for crack problems with non-penetration condition, *Numer. Methods Partial Differential Equations*, to appear.

[11] K. Ito and K. Kunisch, Semi-smooth Newton methods for the variational inequalities of the first kind, *ESAIM, Math. Modelling Numer. Anal.* **37** (2003), 41–62.

[12] A.M. Khludnev and V.A. Kovtunenko, *Analysis of Cracks in Solids*, WIT-Press, Southampton, Boston, 2000.

[13] A.M. Khludnev and J. Sokolowski, The Griffith formula and the Cherepanov-Rice integral for crack problems with unilateral conditions in nonsmooth domains, *Euro. J. Appl. Math.* **10** (1999), 379–394.

[14] D. Klatte and B. Kummer, *Nonsmooth Equations in Optimization*, Kluwer Publishers, Dordrecht, 2002.
[15] M. König, R. Krüger, K. Kussmaul, M. von Alberti, and M. Gädke, Characterizing static and fatigue interlaminar fracture behavior of a first generation graphite/epoxy composite, *13th Composite Materials: Testing and Design* **13**, *ASTM STP 1242*, J.S. Hooper (Ed.), ASTM, 1997, 60–81.
[16] V.A. Kovtunenko, Invariant energy integrals for the non-linear crack problem with possible contact of the crack surfaces, *J. Appl. Maths. Mechs.* **67** (2003), 99–110.
[17] V.A. Kovtunenko, Numerical simulation of the non-linear crack problem with non-penetration, *Math. Meth. Appl. Sci.* **27** (2003), 163–179.
[18] V.A. Kovtunenko, Interface cracks in composite orthotropic materials and their delamination via global shape optimization, Preprint.
[19] S.G. Lekhnitskii, *Theory of Elasticity of an Anisotropic Body*, Holden-Day, San Francisco, 1963.
[20] A. Leontiev, J. Herskovits and C. Eboli, Optimization theory application to splitted plane bending problems, *Int. J. Solids Structures* **35** (1998), 2679–2694.
[21] R. Mifflin, Semismooth and semiconvex functions in constrained optimization, *SIAM J. Control Optim.* **15** (1977), 959–972.
[22] N. Moës, J. Dolbow and T. Belytschko, A finite element method for crack growth without remeshing, *Int. J. Numer. Math. Engng.* **46** (1999), 131–150.
[23] N.F. Morozov, *Mathematical Foundation of the Crack Theory*, Nauka, Moscow, 1984, in Russian.
[24] S.A. Nazarov, The interface crack in anisotropic bodies: stress singularities and invariant integrals, *J. Appl. Maths. Mechs.* **62** (1998), 453–464.
[25] J.R. Rice, Elastic fracture mechanics concepts for interfacial cracks, *Trans. ASME. Ser. E. J. Appl. Mech.* **55** (1988), 98–103.
[26] N. Sukumar, N. Moës, B. Moran and T. Belytschko, Extended finite element method for three-dimensional crack modelling, *Int. J. Numer. Math. Engng.* **48** (2000), 1549–1570.
[27] T.C.T. Ting, Explicit solution and invariance of the singularities at an interface crack in anisotropic composites, *Int. J. Solids Structures* **22** (1986), 965–983.
[28] M. Ulbrich, Semismooth Newton methods for operator equations in function spaces, *SIAM J. Optim.* **13** (2003), 805–842.

5. Appendix

The elasticity coefficients in (2.5) have the form (see [19]):

$$
\begin{aligned}
C_{11}^{\beta} &= C'_{33}\sin^4\beta + 2(C'_{13}+2C'_{66})\sin^2\beta\cos^2\beta + C'_{11}\cos^4\beta,\\
C_{66}^{\beta} &= C'_{66} + (C'_{33}+C'_{11}-2C'_{13}-4C'_{66})\sin^2\beta\cos^2\beta,\\
C_{16}^{\beta} &= \big[C'_{11}\cos^2\beta - C'_{33}\sin^2\beta - (C'_{13}+2C'_{66})(\cos^2\beta-\sin^2\beta)\big]\\
&\quad\times\sin\beta\cos\beta,\\
C_{44}^{\beta} &= C'_{44}\cos^2\beta + C'_{55}\sin^2\beta,\\
C_{55}^{\beta} &= C'_{44}\sin^2\beta + C'_{55}\cos^2\beta,\\
C_{45}^{\beta} &= (C'_{44}-C'_{55})\sin\beta\cos\beta,\\
C_{12}^{\beta} &= C'_{23}\sin^2\beta + C'_{12}\cos^2\beta,\\
C_{26}^{\beta} &= (C'_{12}-C'_{23})\sin\beta\cos\beta,\\
C_{22} &= C'_{22},
\end{aligned}
\tag{5.1}
$$

where the coefficients subscribed with "prime" are related to the rotated coordinate system (x'_1, x'_2, x'_3). They connect the material parameters in (2.1) by the relations:

$$
\begin{aligned}
&C'_{11} = \theta\Big(\frac{1}{E_2} - \frac{\nu_{32}^2}{E_3}\Big), \quad C'_{12} = \theta\Big(\frac{\nu_{21}}{E_2} + \frac{\nu_{31}\nu_{32}}{E_3}\Big),\\
&C'_{13} = \theta\Big(\frac{\nu_{31}+\nu_{21}\nu_{32}}{E_2}\Big), \quad C'_{22} = \theta\Big(\frac{1}{E_1} - \frac{\nu_{31}^2}{E_3}\Big),\\
&C'_{23} = \theta\Big(\frac{\nu_{32}}{E_1} + \frac{\nu_{21}\nu_{31}}{E_2}\Big), \quad C'_{33} = \theta\frac{E_3}{E_2}\Big(\frac{1}{E_1} - \frac{\nu_{21}^2}{E_2}\Big),\\
&C'_{44} = G_{21}, \quad C'_{55} = G_{32}, \quad C'_{66} = G_{31},\\
&\frac{1}{\theta} = \Big(\frac{1}{E_2} - \frac{\nu_{32}^2}{E_3}\Big)\Big(\frac{1}{E_1} - \frac{\nu_{31}^2}{E_3}\Big) - \Big(\frac{\nu_{21}}{E_2} + \frac{\nu_{31}\nu_{32}}{E_3}\Big)^2.
\end{aligned}
\tag{5.2}
$$

As specific case we suppose throughout that the material parameters (2.1) satisfy the identities:

$$
\begin{aligned}
&E_1 = E_2 = E, \quad \nu_{21} = \nu, \quad G_{21} = \frac{E}{2(1+\nu)},\\
&\nu_{31} = \nu_{32} = \nu_3, \quad G_{31} = G_{32} = G_3,
\end{aligned}
\tag{5.3}
$$

thus reducing the number of independent material parameters to 5. These parameters describe a fibering along the x'_3-axis of a material which is isotropic in every plane $x'_3 = const$. With (5.3) we can rewrite

(5.2) in the form:

$$
\begin{aligned}
&C'_{11} = C'_{22} = \kappa\frac{E}{1+\nu}\Big(\frac{1}{E} - \frac{\nu_3^2}{E_3}\Big), \quad C'_{12} = \kappa\frac{E}{1+\nu}\Big(\frac{\nu}{E} + \frac{\nu_3^2}{E_3}\Big),\\
&C'_{13} = C'_{23} = \kappa\nu_3, \quad C'_{33} = \kappa\frac{E_3}{E}(1-\nu),\\
&C'_{44} = \frac{E}{2(1+\nu)}, \quad C'_{55} = C'_{66} = G_3,\\
&\frac{1}{\kappa} = \frac{1-\nu}{E} - \frac{2\nu_3^2}{E_3} = \Big(\frac{1}{E} - \frac{\nu_3^2}{E_3}\Big) - \Big(\frac{\nu}{E} + \frac{\nu_3^2}{E_3}\Big).
\end{aligned} \tag{5.4}
$$

Note that the coefficients in (5.4) fulfill the relations:

$$
C'_{12} + 2C'_{44} = C'_{11} = C'_{22}, \quad C'_{12} + C'_{44} = 0.5\kappa. \tag{5.5}
$$

In what follows we consider the two limit cases $\beta = 0$ and $\beta = \pm\pi/2$. For $\beta = 0$ we introduce the Lamé parameters:

$$
\mu = \frac{E}{2(1+\nu)}, \quad \lambda = \kappa\frac{E}{1+\nu}\Big(\frac{\nu}{E} + \frac{\nu_3^2}{E_3}\Big). \tag{5.6}
$$

In this case, from (5.5) and (5.6) we obtain that $\kappa = 2(\lambda+\mu)$ and the coefficients in (5.1) are the following:

$$
\begin{aligned}
&C^0_{11} = C_{22} = \lambda + 2\mu, \quad C^0_{12} = \lambda, \quad C^0_{44} = \mu,\\
&C^0_{55} = C^0_{66} = G_3, \quad C^0_{16} = C^0_{26} = C^0_{45} = 0.
\end{aligned} \tag{5.7}
$$

Using (5.7) the stress in (2.6) is split into the components for $(u_1, u_2)^\top$:

$$
\begin{aligned}
\sigma^0_{11}(u) &= C^0_{11}u_{1,1} + C^0_{12}u_{2,2},\\
\sigma^0_{22}(u) &= C^0_{12}u_{1,1} + C_{22}u_{2,2},\\
\sigma^0_{12}(u) &= C^0_{44}(u_{1,2} + u_{2,1}),
\end{aligned} \tag{5.8}
$$

and independent components for u_3:

$$
\sigma^0_{23}(u) = C^0_{55}u_{3,2}, \quad \sigma^0_{13}(u) = C^0_{66}u_{3,1}. \tag{5.9}
$$

Hence from (5.8) and (5.9) we arrive at a 2-dimensional Lamé/ Laplace operator in (2.9) for the in-plane/ anti-plane isotropic problem:

$$
\begin{aligned}
\sigma^0_{1\alpha,\alpha}(u) &= \mu\Delta u_1 + (\lambda+\mu)(\operatorname{div} u)_{,1},\\
\sigma^0_{2\alpha,\alpha}(u) &= \mu\Delta u_2 + (\lambda+\mu)(\operatorname{div} u)_{,2},\\
\sigma^0_{3\alpha,\alpha}(u) &= G_3\Delta u_3,
\end{aligned}
$$

where $\operatorname{div} u = u_{1,1} + u_{2,2}$ and $\Delta u_i = u_{i,11} + u_{i,22}$, $i = 1, 2, 3$.

Next consider the case $\beta = \pm\pi/2$. From (5.1) and (5.3) we derive that

$$
\begin{aligned}
&C_{11}^{\pm\pi/2} = \kappa\frac{E_3}{E}(1-\nu), \quad C_{22} = \kappa\frac{E}{1+\nu}\Big(\frac{1}{E} - \frac{\nu_3^2}{E_3}\Big),\\
&C_{12}^{\pm\pi/2} = \kappa\nu_3, \quad C_{55}^{\pm\pi/2} = \frac{E}{2(1+\nu)}, \quad C_{44}^{\pm\pi/2} = C_{66}^{\pm\pi/2} = G_3,\\
&C_{16}^{\pm\pi/2} = C_{26}^{\pm\pi/2} = C_{45}^{\pm\pi/2} = 0.
\end{aligned}
\tag{5.10}
$$

According to (5.10) the stress tensor (2.6) is split similarly to (5.8) and (5.9). As a result we arrive at the following operator in (2.9) for the in-plane/ anti-plane orthotropic problem:

$$
\begin{aligned}
\sigma_{1\alpha,\alpha}^{\pm\pi/2}(u) &= \kappa\frac{E_3}{E}(1-\nu)u_{1,11} + G_3u_{1,22} + (\kappa\nu_3 + G_3)u_{2,12},\\
\sigma_{2\alpha,\alpha}^{\pm\pi/2}(u) &= (\kappa\nu_3 + G_3)u_{1,12} + G_3u_{2,11} + (2\mu+\lambda)u_{2,22},\\
\sigma_{3\alpha,\alpha}^{\pm\pi/2}(u) &= G_3u_{3,11} + \mu u_{3,22}.
\end{aligned}
$$

We can conclude that the spatial model under consideration is intermediate between the plane isotropic model for $\beta = 0$ and the plane orthotropic model for $\beta = \pm\pi/2$.